博士学位論文

Dielectric α relaxation of supercooled sugar alcohols

(過冷却糖アルコールの誘電 α 緩和)

川谷維摩

北海道大学大学院理学院

物性物理学専攻

2024 年 3 月

Contents

Abstract

Glass transition phenomena is one of the most important problem of physics. Investigation of supercooled liquids is useful to clarify phenomena related to glass transitions. It has been pointed out in several literatures that dielectric α process doesn't follow the Vogel-Fulcher-Tammann (VFT) equation near T_g even the experiments had been performed under the condition where the sample system is well relaxed to thermodynamic equilibrium state. It is necessary to investigate whether the glass transition is simply a relaxation phenomenon due to the finite observation time, or it is some kind of transition where a change in dynamics occurs. It is considered that such claims have been increased after accessible frequency range of dielectric spectroscopy had attained low frequencies such as sub-milli Hz region. In this case, it is concerned that the thermodynamical condition meets well-relaxed equilibrium state. In this study, we re-examine the behavior of the α process using typical glass formers sorbitol, xylitol and glycerol in an extremely wide frequency from 110 MHz down to 10 μHz paying attention to the thermal history of the sample during the entire measurements to precise measurement. It is found that the behavior of the α process in sorbitol depends on the thermal history. Near T_g, the α process doesn't follow the VFT equation derived from experimental data well above T_g. This indicates that the α process cannot be represented by a simple function from high temperature to low temperature just above the glass transition temperature. However, the divergence manner of the α relaxation frequency at a finite temperature is kept even near T_g. The results suggest that the glass transition is not just a relaxation phenomenon but some kind of transition with a changing dynamics.

This article is devided into five chapters. In chapter 1, we will give you an overview of reserch on supercooled liquids and glass transitions, and the motivation for this study will be presented. In chapter 2, we recall the basic knowledge of dielectric relaxation phenomena to helping discussions in following chapters. In chapter 3, the effect of electrode structure on relaxation frequency is examined. In chapter 4, we will discuss the effect of thermal history on the relaxation frequency. Chapter 5 contains the conclusion of this thesis.

Chapter 1

Introduction

1.1 Glass transition and supercooled liquids

Glass transition phenomena is one of the most important problem of physics. Despite the long-term efforts of many researchers, that is still not understood well. We have addressed the question of whether the glass transition phenomenon is an apparent transition due to the finite observation time or a true transition by precisely measuring the α process of undercooled liquids using dielectric spectroscopy.

The glass transition phenomenon occurs when a liquid is cooled. Here, we review liquids, crystals and glasses. Figure 1.1 shows the schematic picture of the glass transition. Normally, when a liquid is cooled down, it will crystallize at the melting point T_{m}. However, when the cooling rate is set higher, the liquid may not crystallize even below T_{m}. Such liquids are called supercooled liquids. When the temperature of the super cooled liquid is further lowered, the rate of volume change decreases at a certain temperature T_{g}, and the liquid will solidify. At the same time, the viscosity of the supercooled liquid increases drastically. Such a change of state that occurs after T_{g} is called glass transition, and T_{g} is called the glass transition temperature. If the glass transition occurs at T_{g1} when a liquid is cooled at a certain cooling rate, a glass transition occurs at lower temperature T_{g2} when the liquid is cooled at slower cooling rate. The supercooled state is quasi-equilibrium state, the glass transition phenomenon depends on the thermal history, such as cooling rate, therefore the glassy state is thermodynamically nonequilibrium. In addition, glass transition is different from crystal-

lization. Crystallization is a phase transition with a well defined thermodynamic transition temperature, while glass transition is a dynamical phenomenon in which the timescale of molecular motion is longer than the experimental timescale. Furthermore, from a molecular perspective, glass is an amorphous solid and does not have the long-range order like crystals.

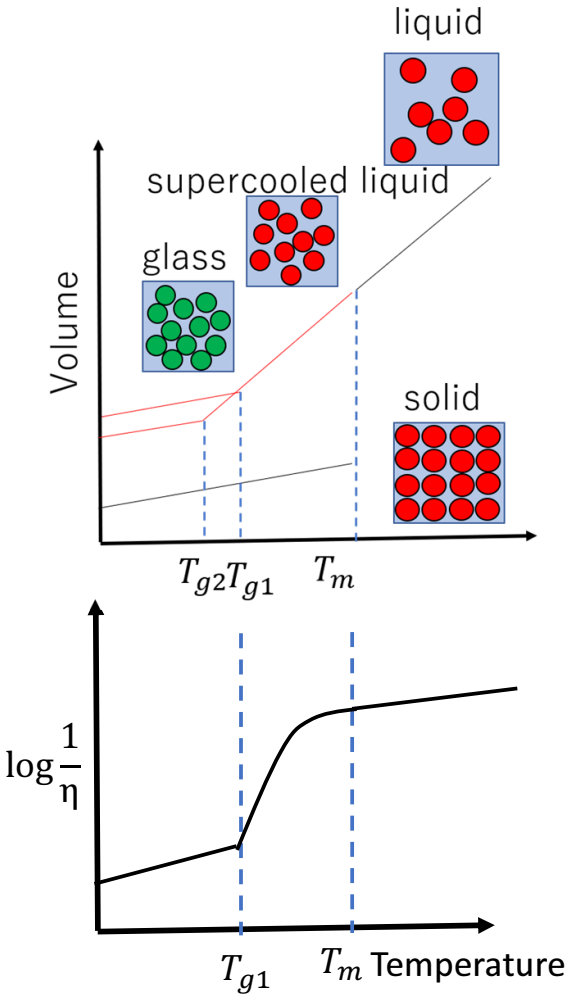

Figure 1.1: Schematic picture of the glass transition. The upper figure shows the temperature dependence of the volume of a material. The glass transition temperature is generally defined by the point at which the slope changes. In the lower figure, the vertical axis is the logarithm of the inverse of the viscosity. The viscosity of a supercooled liquid increases dramatically with decreasing temperature.

1.2 α relaxation near the glass transition temperature

Whenever a liquid vitrifies, it passes through a supercooled liquid which is a sub-equilibrium state, and the vitrification can be regarded as the glass transition of the supercooled liquid. Therefore, investigating the behavior of supercooled liquids near the glass transition temperature is a useful tool for studying glass transitions. Since the glass transition phenomenon is related to viscosity, it is possible to measure it directly.However, this approach has the disadvantage of a narrow frequency range that can be observed. The time scales of molecular motions related to the glass transition are wide, so that Broadband Dielectric Spectroscopy (BDS) is one of the most suitable techniques to investigate such phenomena. Figure 1.2 shows a typical frequency dependence of the dielectric loss of a glass forming material obtained by BDS. From the low frequency side, several relaxation processes are observed: α process, JG-β process. In particular, the dielectric α relaxation is sensitive to temperature, so that it is considered that it corresponds to the drastic increase in viscosity associated with the glass transition.

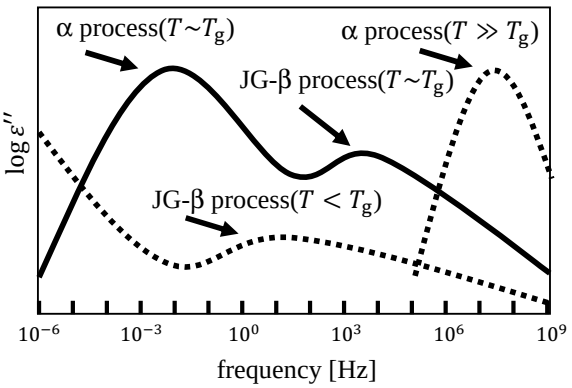

Figure 1.2: Schematic picture of dielectric dispersion. The α process appears on the high-frequency side if the temperature is sufficiently higher than T_g and drastically shifts to the low-frequency side as the temperature decreases.

The frequency at which dielectric loss peak is called the dielectric relaxation frequency f_m. The temperature dependence of the dielectric relaxation frequency is shown in Figure 1.3. The relaxation process is divided into two processes at temperature T_M, that is, α and JG-β

processes. Relaxation frequency of β process shows Arrhenius type temperature dependence and α process shows non-Arrhenius type one.

Such a non-Arrhenius behavior is often represented by use of empirical formulas Vogel-

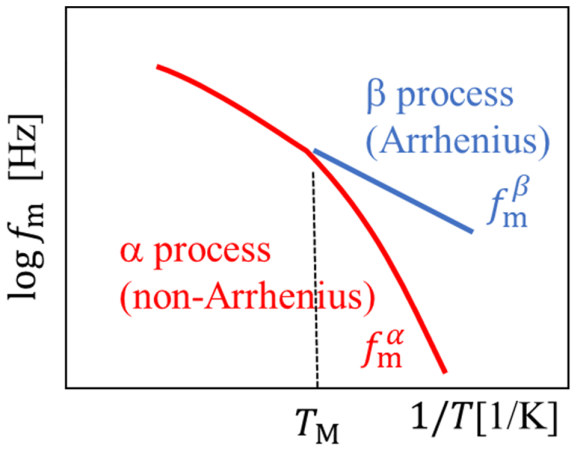

Figure 1.3: Schematic relaxation map. The horizontal axis is the reciprocal temperature. This is so-called Arrhenius plot. The behavior following the Arrhenius formula is represented by a straight line in the figure.

Fulcher-Tammann (VFT) equation [1–3] or Williams-Landel-Ferry (WLF) equation [4]. The VFT equation is given as

$$\log f_{\mathrm{m}}^{\alpha} = A - \frac{B}{T - T_0}, \tag{1.1}$$

where f_{m}^{α} is relaxation frequency of the α process, A, B and T_0 are parameters. The characteristic feature of this equation is that the relaxation frequency diverges at a finite temperature T_0. This equation is explained by Adam-Gibbs theory which is described in the next section.

1.3 Adam-Gibbs theory

In this section, we introduce the Adam-Gibbs theory (AG theory) [5], which is one of the theories to explain the increase of viscosity at low temperatures. This theory can provide the VFT feature. In this theory, cooperatively rearranging region (CRR) is defined as a microscopic origin of the α relaxation. The CRR corresponds the smallest region in which molecules move cooperatively. A schematic image of CRR is shown in Figure 1.4 [6]. Size

of the CRR increases as temperature decreases toward T_g as shown in Figure 1.5. Using this concept, we can derive a theoretical equation that is identical to the experimental VFT equation.

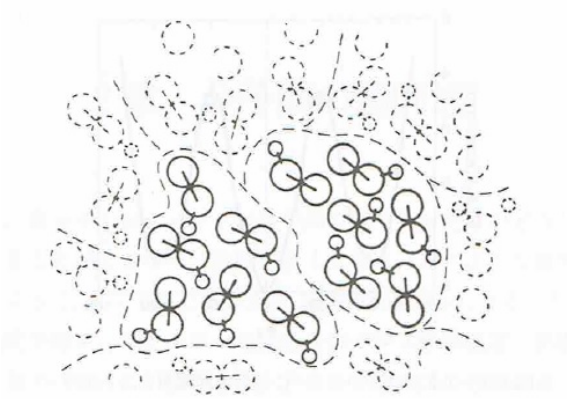

Figure 1.4: Schematic picture of CRR. [6]

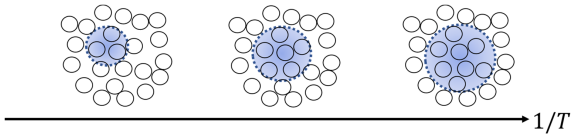

Figure 1.5: Schematic picture of temperature dependence of CRR size.

The potential energy barrier E_a for all z molecules in a CRR to rearrange can be written as

$$E_a = z\Delta\mu \tag{1.2}$$

using the potential energy of single molecule hindering rearrangement, $\Delta\mu$.
Here, the probability of the transition of the CRR, $W_0(T)$ is given by

$$W_0(T) = A\exp\left(\frac{-z\Delta\mu}{kT}\right). \tag{1.3}$$

Let z^* be the number of molecules in the smallest CRR, the average transition probability can be discribe as

$$\bar{W}_0(T) = \bar{A}\exp\left(\frac{-z^*\Delta\mu}{kT}\right). \tag{1.4}$$

Using S_c for the configurational entropy of a macroscopic sample, N_A for the Avogadro number, and S_c^* for the configurational entropy of the smallest CRR, we can obtain the following relationship with Z^*. The schematic picture about the configurational entropy is shown in Figure 1.6.

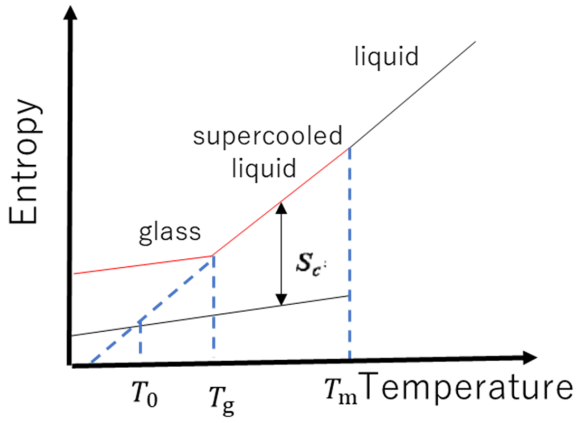

Figure 1.6: Consept of the configurational entropy.

$$z^* = \frac{N_A s_c^*}{S_c} \tag{1.5}$$

Using this formula, the average transition probability can be written as

$$\bar{W}_0(T) = \bar{A} \exp\left(\frac{-s_c^* N_A \Delta\mu}{T S_c}\right). \tag{1.6}$$

The S_c can be calculated by $\Delta C_p = C_{p(\text{liquid})} - C_{p(\text{glass})}$. That is,

$$S_c = \int_{T_0}^{T} \frac{\Delta C_p}{T} dT. \tag{1.7}$$

Where, T_0 is the temperature such that $S_c = 0$. Experimental facts support the approximation with a constant α, $\Delta C_p = \alpha/T$. Therefore,

$$S_c = \frac{\alpha(T - T_0)}{T_0 T} \tag{1.8}$$

and finally we can obtain

$$\bar{W}(T) = \bar{A} \exp\left(\frac{-DT}{T - T_0}\right). \tag{1.9}$$

Where $D = C/\alpha$. This is consistent with empirical VFT equation describing the temperature dependence of the α relaxation frequency.

1.4 α relaxation near T_g

Although the VFT equation has succeed in many glass forming materials in the temperature region well above T_g, there are reports finding that the temperature dependence of the α process near T_g ($T > T_g$) deviates from the VFT equation which is determined by high temperature range. We have studied dielectric relaxation behavior of many supercooled liquids by employing experimental setups of broad-band dielectric spectroscopy essentially developed by our research group [7–14].

We have already reported that the temperature dependence of f_m^α of poly (vinyl acetate) (PVAc) near T_g deviates from the VFT equation obtained from data well above T_g [15] (Figure 1.7). In that report, there is deviations of the relaxation frequency to the lower frequency side than predicted by the VFT near T_g. It was noted that that could be described by the Arrhenius equation.

On the other hand, the other study of the dielectric measurement for PVAc also suggests a deviation of the shift factor (a_T) which corresponds to relaxation time from the VFT equation near T_g [16] (Figure 1.8). However, these deviations from the VFT equation reported there are found to be in opposite directions. Contradictory results were obtained even for the same material.

We have also reported similar dielectric measurements on sorbitol [14] (Figure 1.9). In this report, deviation of the temperature dependence of f_m^α from the VFT feature was found near T_g. The direction of data deviation is lower frequency side than VFT prediction using data well above T_g.

Several other studies [18–20] suggest that the experimental data of the α process which is closely related to the glass transition does not follow the VFT equation near T_g. An example of that is shown in Figure 1.10. It is considered that clarifying this break of the VFT feature is important for understanding the mechanism of the glass transition. Novikov and Sokolov [21] pointed out that it is important question that whether there is a divergence of the structural relaxation time scale at a finite temperature below T_g and the current experimental data do

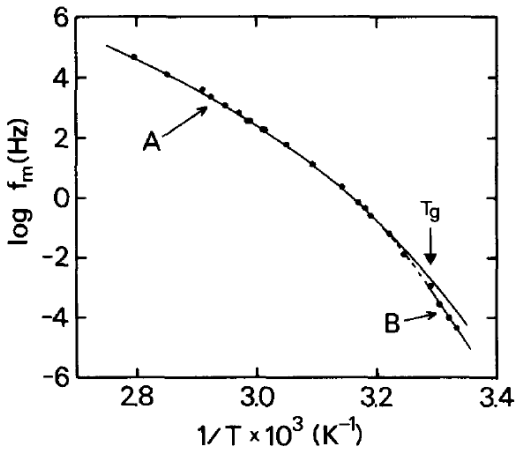

Figure 1.7: Temperature dependence of relaxation time of PVAc. Dots are measured values, line A shows VFT fitting at high temperature, and line B shows Arrhenius fitting below T_g.

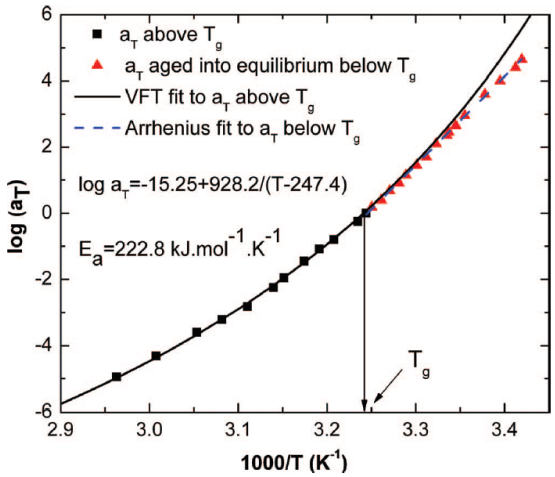

Figure 1.8: Temperature dependence of relaxation time of PVAc. Squares indicate relaxation times above T_g, triangles indicate T relaxation times below $_g$, solid lines indicate VFT fitting above T_g, and dotted lines indicate Arrhenius fitting below T_g.

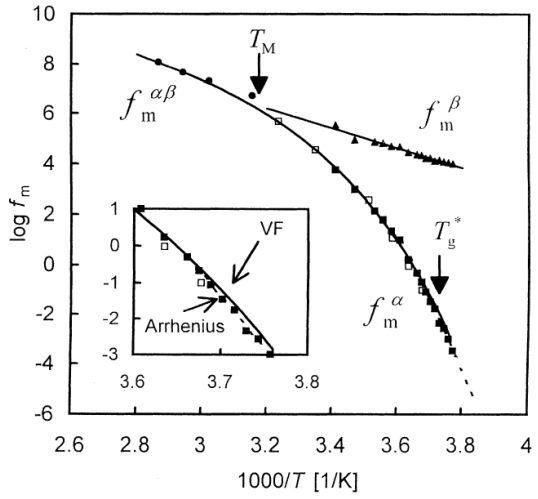

Figure 1.9: Sorbitol relaxation map. Black squares indicate log f_{m}^{α}, black triangles indicate log f_{m}^{β}, black circles indicate log $f_{\mathrm{m}}^{\alpha\beta}$, white squares indicate data The white squares indicate the data of [17]

not provide an unambiguous answer, and the theoretical models suggest both scenarios.

Some reports indicate that fitting is possible using multiple VFT equations from high to low temperatures [22, 23]. So-called stickel plot of the viscosity data of TNB (Figure 1.11) shows that the data represented by an Arrhenius type equation and two VFT equations which have different parameters.

1.5 Motivation of this study

As described above, in recent years, more and more reports have suggested that the glass transition may be some kind of transition rather than the apparent transition due to the finite observation time. On the other hand, the reproducibility of the results is not sufficient. It is necessary to measure samples in a quasi-equilibrium state, however, previous studies have not paid sufficient attention to this point.

From the experimental point of view, there are several things which can be cause of such discrepancies. One is that polymers may not be suitable materials to investigate the α dynamics

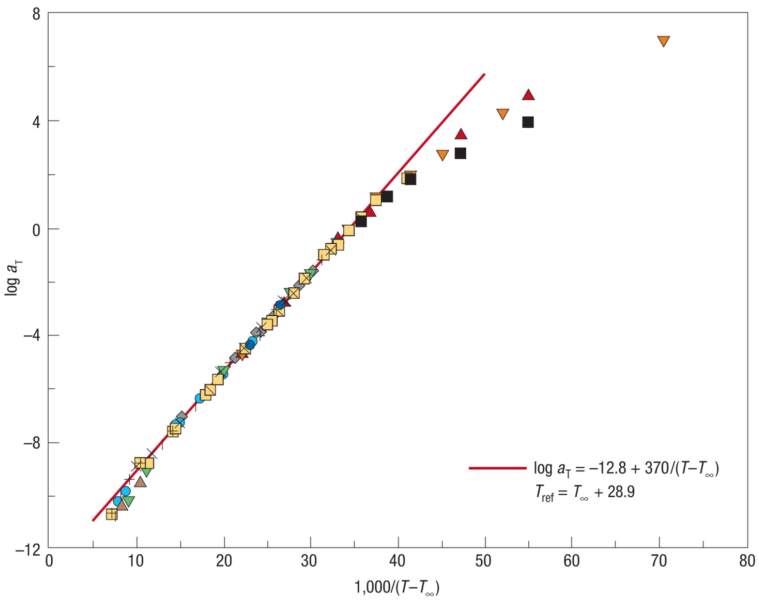

Figure 1.10: Relaxation data as shift factors a_{T} for polystyrene [19]. In this figure, the horizontal axis is set to $1000/(T - T_\infty)$ so that the behavior following the VFT is linear.

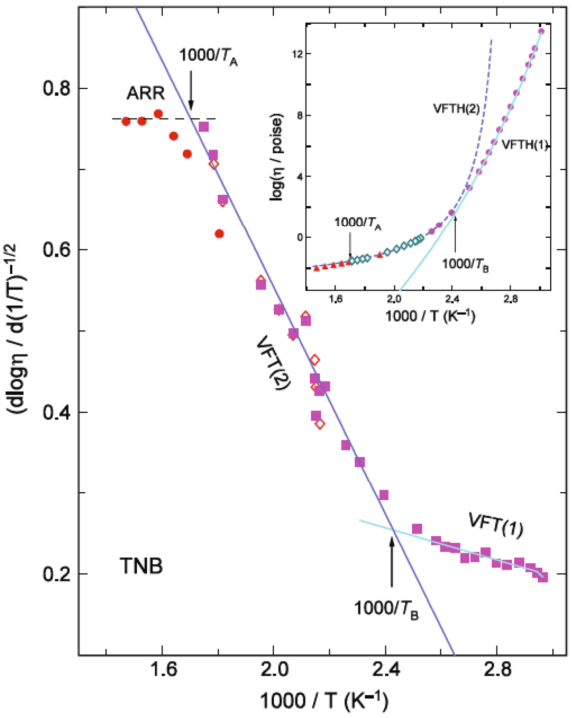

Figure 1.11: Stickel plot of the viscosity data of TNB [22, 23].

near T_g. While polymers are often used for such experiments in order to investigate molecular dynamics of supercooled materials because atactic polymers don ' t undergo crystallization with variety of thermal history. However, there is concern about unexpected effects due to entanglement especially in the glass transition temperature region [24].

The second, this is the most important point, is thermal history during dielectric measurements. As has been indicated in the volume relaxation experiments by Kovacs et al. [25, 26] (Figure 1.12 and 1.13), careful control of the thermal history is required to attain thermal equilibrium conditions, and such experiments are time-consuming especially near T_g. It is important to observe behavior of the α process of supercooled liquids under thermodynamically relaxed conditions.

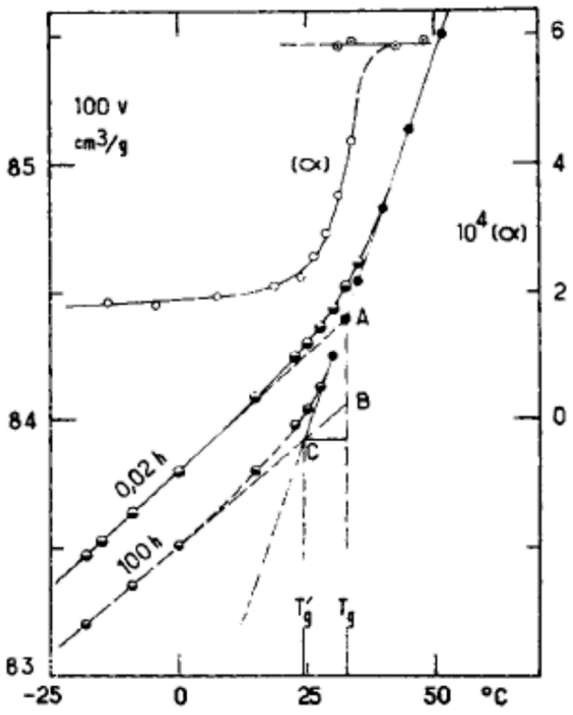

Figure 1.12: Volume relaxation for PVAc. Samples with different cooling rates have different glass transition temperatures. Compare samples cooled from high temperature for 0.02 hours to samples cooled for 100 hours, smaller cooling rate results lower T_g.

The third one is on mechanical condition of the sample being measured in a dielectric cell. Generally, in the case of the measurement for a sample which have high fluidity when that is

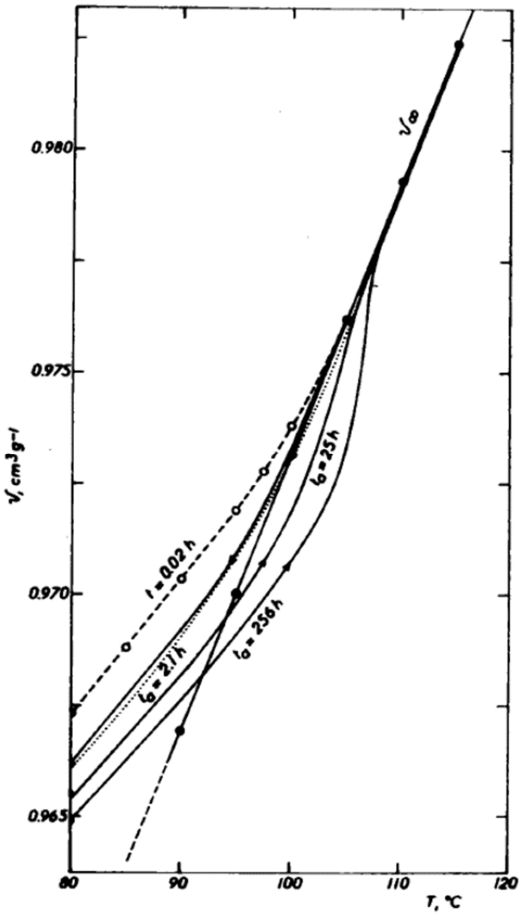

Figure 1.13: Volume relaxation for polystyrene. Samples isothermally annealed 2.1, 25, 256 hours at 80° after cooling from high temperature for 0.02 hours below T_{g} show relaxation toward a quasi-equilibrium state. In addition, each reheated sample becomes an equilibrium liquid through different paths.

installed in a measurement cell, the experiment performed using a cell with fixed electrode spacing. In this case, the volume reduction of the sample with temperature decreasing may be prohibited. There is concern that cooling a liquid sample in such rigid cell with no change in spacing may cause negative pressure. This may restrict change of density and can be cause of large error in estimating the value of f_{m}^{α}.

In this study, we performed dielectric measurement of supercooled poly-hydric alcohols (sorbitol, xylitol and glycerol) in the frequency range 10 μHz to 110 MHz to investigate the temperature dependence of the α relaxation frequency in wide temperature range including near T_{g} under the experimental condition paying sufficient attention to the thermal history to precise measurement.

The results show that the difference in thermal history has a large effect to the α relaxation frequency. We found that f_{m}^{α} of sorbitol strongly depends on cooling rate in lower temperature range especially near T_{g}. In contrast to this effect, the difference from the electrode condition is very small. On the other hand, the α process of well relaxed supercooled sorbitol doesn ' t follow the VFT equation derived from the experimental data well above T_{g}. In other words, the α process cannot be described by a single function over the entire temperature range, including just above the glass transition temperature. Even in this case, however, the divergence manner of the α relaxation frequency in a finite temperature is kept even near T_{g}. These results suggest the divergence feature of the relaxation frequency is essential, however, the f_{m}^{α} feature is not so simple as is explained by simple theory such as classical AG theory. Furthermore, the change in the $f_{\mathrm{m}}^{\alpha}(T)$ may indicate that the glass transition is not just a relaxation phenomenon but a transition involves some change in dynamics.

Chapter 2

Experiment

2.1 Dielectric relaxation and complex dielectric constant

For the discussion in following chapters, we recall the basic knowledge of dielectric relaxation phenomena in this section. Some books [27–29] are helpful so that we summarize the dielectric relaxation phenomenon and BDS refering them.

2.1.1 Dielectric constant

When we apply a voltage V for a capacitor consists of two parallel conductive plates filled with a dielectric, a charge of $+Q$ is placed on one plate and $-Q$ on the other plate and the capacitance C is defined as

$$Q = \frac{C}{V}. \tag{2.1}$$

Generally, C can be described as

$$C = \varepsilon K, \tag{2.2}$$

where, K is a constant which can be calculated from the geometric arrangement of the electrodes and ε is the permittivity. When the dielectric is replaced with a vacuum,

$$C_0 = \varepsilon_0 K, \tag{2.3}$$

where, the permittivity of vacuum, $\varepsilon_0 = 8.855 \times 10^{-12}$[F/m] and the capacitance with vacuum, C_0. Here, we define the dielectric constant, ε_r as

$$\frac{\varepsilon}{\varepsilon_0} = \varepsilon_\mathrm{r}. \tag{2.4}$$

Here, we consider a parallel plate cell as an example. We can obtain K in the equation(2.2).

$$K = \frac{A}{d}, \tag{2.5}$$

where, the area of the electrode is A, and the distance between the electrodes is d. Substitute equations (2.2) and (2.5) into equation (2.1),

$$\frac{Q}{A} = \varepsilon \frac{V}{d}. \tag{2.6}$$

Here, q is the surface density of the electrode charge and E is the strength of the electric field,

$$q = \varepsilon E. \tag{2.7}$$

2.1.2 Polarization

When a dielectric is placed in an electrostatic field, the positive charges in the atoms and molecules of the dielectric material are displaced in the direction of the electric field and the negative charges in the opposite direction, and inducing dipole moments. This state is called the polarization of an electron or molecule, and the dipole moment induced by the electric field is called the induced dipole moment. When atoms or molecules in the dielectric are polarized, charges have the opposite sign that of the electrode appears on the surface of the dielectric. This state is called dielectrics are polarized, and the charge is called polarized charge or bound charge. On the other hand, the charges that are originally present in the electrode is called true charge, and the charge that is responsible for the formation of the electric field is called free charge. The vector $\boldsymbol{P}$, whose magnitude is equal to the amount of charge passing through a unit area perpendicular to the electric field E in a dielectric material and whose direction is the same as the electric field, is called the polarization. Polarization is closely related to dielectric constant.

We consider an electric flux density $\boldsymbol{D}$. Its direction coincides with that of the electric field and its magnitude is equal to the true charge, $D = q$. The relation

$$\boldsymbol{D} = \varepsilon_r \varepsilon_0 \boldsymbol{E} = \varepsilon_0 \boldsymbol{E} + \boldsymbol{P} \tag{2.8}$$

is established between the dielectric constant and the polarization. That is,

$$\varepsilon_r - 1 = \frac{\boldsymbol{P}}{\varepsilon_0 \boldsymbol{E}} \equiv \chi. \tag{2.9}$$

The χ is called the electrosensitivity. The larger the electrosensitivity, the larger the dielectric constant.

Polarization phenomena in homogeneous dielectrics can be roughly classified into three types based on the behavior of atoms or molecules: electronic polarization, atomic polarization, and dipole polarization. Electronic polarization is a polarization based on the change in the relative position of the electron cloud of an atom with respect to the nucleus. Atomic polarization is based on the change in the relative positions of positively charged and negatively charged atoms, such as positive and negative ions in an ionic crystal. Dipole polarization is a polarization based on the orientation of dipole moments of polar molecules. Without an electric field, the dipole moments of polar molecules in a material would be oriented in different directions due to thermal motion, and there would be no polarization of the material as a whole. However, when an electric field acts on the dipole moments, the dipole moments are torqued and tend to change their orientation in the direction of the electric field against the thermal motion. As a result, the dipole moment is induced in the electric field direction and polarization occurs for the whole substance. Electron polarization and atomic polarization are called displacement polarization because they are caused by the displacement of positive and negative charge, and dipole polarization is also called orientation polarization because it is caused by the orientation of dipole moments in the electric field direction.

It takes a certain amount of time for the polarization to reach an equilibrium state when an electric field actually acts on the material. The speed of polarization formation corresponds to the speed of electronic and atomic oscillation in the case of electronic and atomic polarization, respectively, so that polarization is formed almost instantaneously. Therefore, these polarizations are also called instantaneous polarizations. When the electric field is removed,

they disappear through the reverse process. In the case of dipolar polarization, on the other hand, it takes a relatively long time for the polarization to reach an equilibrium state because the action of an electric field causes the surrounding molecules to prevent the dipole moment from moving in an oriented manner. On the contrary, when the electric field is removed, the polarization gradually disappears. This phenomenon is called dielectric relaxation. When the electric field is not strong, the polarization change during discharge is consistent with the reverse of that during charging. This property is called reversible property, and a dielectric with this property is called a linear dielectric. The time required for the polarization to decrease to $1/e$ of the equilibrium state after the electric field is removed is called the relaxation time.

Since actual polarized materials exhibit both of the above polarizations, the time variation of polarization is as shown in Fig.2.1. Since the polarization changes with time after an electric field is applied, we must consider that the dielectric permittivity also changes with time.

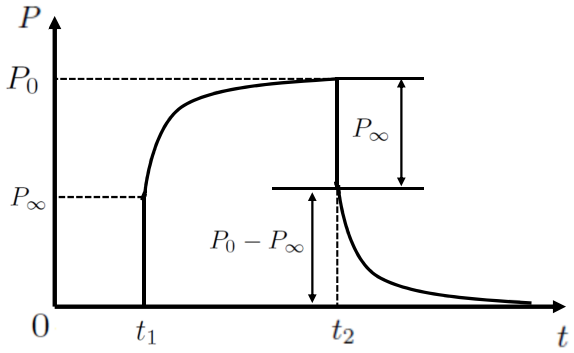

Figure 2.1: Time variation of polarization. When an electric field is applied to the dielectric at time t_1, instantaneous polarization P_∞ occurs, and further orientation polarization occurs, approaching P_0 asymptotically. If the dielectric is a linear dielectric, removing the electric field at time t_2 causes the polarization to become zero by the reverse process.

2.1.3 Complex permittivity

When an alternating voltage

$$V = V_0 e^{i\omega t} \tag{2.10}$$

of the angular frequency $\omega = 2\pi f$ (where f is the frequency) is applied to a vacuum capacitor which has the capacitance C_0, a charging current

$$I_{c0} = i\omega C_0 V \tag{2.11}$$

flows with a phase advance of 90 degrees relative to the applied voltage. Next, we consider the case where a dielectric is filled instead of a vacuum. Since there is a time delay in polarization, the total current $\boldsymbol{I}$ flowing through this dielectric capacitor is delayed in phase by δ than I_{c0}. Therefore, we can discribe

$$\boldsymbol{I} = I_l + I_c = G\boldsymbol{V} + i\omega C\boldsymbol{V} = (G + i\omega C)\boldsymbol{V} \tag{2.12}$$

as the sum of the charging current component I_c and the loss current component I_l (see figure 2.2). A capacitor containing a dielectric can be replaced by an equivalent parallel circuit (see

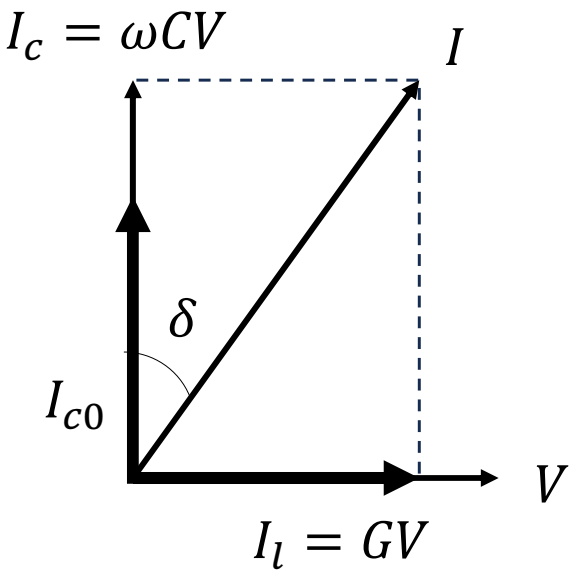

Figure 2.2: Relation between voltage and current.

figure 2.3), where G is called the equivalent parallel conductance and C the equivalent parallel capacitance. Here, using

$$C = \varepsilon'_r C_0 \tag{2.13}$$

and

$$\tan\delta = \frac{|I_l|}{|I_c|} = \frac{G}{\omega C}, \tag{2.14}$$

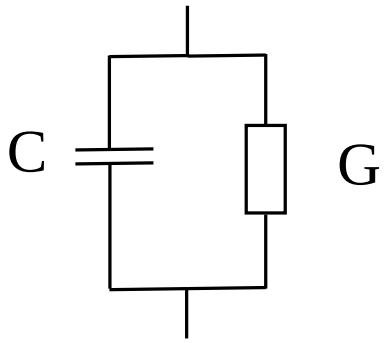

Figure 2.3: Equivalent parallel circuit.

we obtain

$$\boldsymbol{I} = (i\omega\varepsilon'_{\mathrm{r}}C_0 + \omega\varepsilon'_{\mathrm{r}}C_0 \tan\delta)\boldsymbol{V} \tag{2.15}$$

and applying following equations

$$\varepsilon^* = \varepsilon' - j\varepsilon'', \tag{2.16}$$

$$\varepsilon^*_{\mathrm{r}} = \frac{\varepsilon^*}{\varepsilon'} = \varepsilon'_{\mathrm{r}} - i\varepsilon''_{\mathrm{r}}, \tag{2.17}$$

and

$$\tan\delta \equiv \frac{\varepsilon''}{\varepsilon'} = \frac{\varepsilon''_{\mathrm{r}}}{\varepsilon'_{\mathrm{r}}}, \tag{2.18}$$

the relation

$$\boldsymbol{I} = (i\omega\varepsilon'_{\mathrm{r}} + \omega\varepsilon''_{\mathrm{r}})C_0\boldsymbol{V} = i\omega\varepsilon^*_{\mathrm{r}}C_0\boldsymbol{V} \tag{2.19}$$

is lead. And then

$$Y = \frac{\boldsymbol{I}}{\boldsymbol{V}} = i\omega\varepsilon^*_{\mathrm{r}}C_0. \tag{2.20}$$

The complex permittivity $\varepsilon^*_{\mathrm{r}}$ is obtained from the admittance Y. This is the principle of the method of the experimental apparatuses used in this study. Here, ε^* is the complex permittivity, ε^*_r is the complex relative permittivity (in case of no confusion, this may be simply called the permittivity), ε'' is the dielectric loss, $\varepsilon''_{\mathrm{r}}$ is the relative dielectric loss (in case of no confusion, this may be simply called the dielectric loss).

2.1.4 Relaxation phenomena and complex permittivity

The relation between dielectric relaxation and dielectric loss in an AC electric field is discussed here for linear dielectrics. A voltage is applied to the capacitor as shown in figure 2.4.

Then, the charge stored in the capacitor becomes as shown in Figure 2.5.

The charge Q_1 that changes instantaneously during charging and discharging is called in-

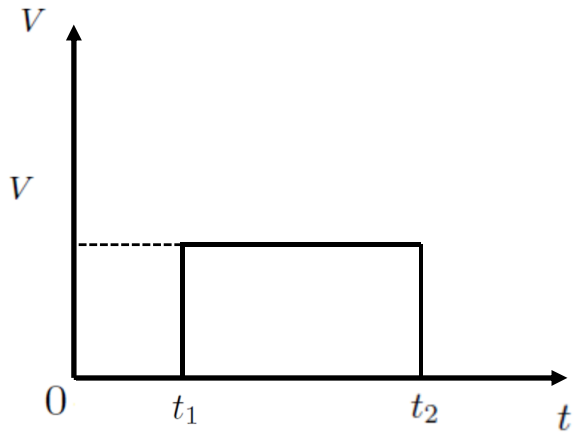

Figure 2.4: Time variation of applied voltage

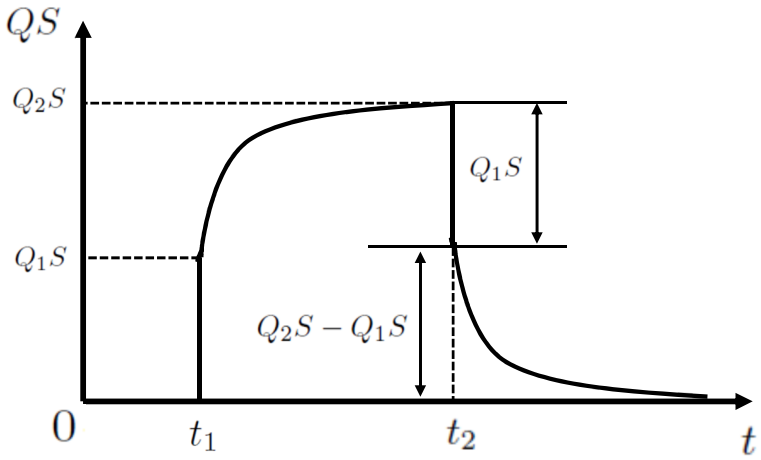

Figure 2.5: Time variation of charging charge

stantaneous charge, the charge that increases with time during charging is called absorbed charge, and the charge that decreases with time during discharging is called residual charge. Absorbed charge and residual charge are the charges due to polarization with dielectric relaxation. Let $Q_{\mathrm{d}}(t)$ be the absorbed charge, and

$$Q = Q_1 + Q_{\mathrm{d}}(t) \tag{2.21}$$

be the total charge when charging. Let C_1 be the capacitance corresponding to the instantaneous charge Q_1 and $\varepsilon_{r\infty}$ be the relative permittivity, and let C_2 be the capacitance corresponding to the total charge Q_2 after polarization formation and ε_{r0} be the relative permittivity, then

$$Q_1 = C_1 V = \varepsilon_{r\infty} C_0 V \tag{2.22}$$

$$Q_2 = C_2 V = \varepsilon_{r0} C_0 V. \tag{2.23}$$

$Q_d(t)$ can written as

$$\begin{aligned} Q_d(t) &= (C_2 - C_1) f(t) V \\ &= (\varepsilon_{r0} - \varepsilon_{r\infty}) C_0 f(t) V. \end{aligned} \tag{2.24}$$

Here, C_0 is the capacitance, $f(t)$ is a function ($f(0) = 0, f(\infty) = 1$) that varies monotonically from 0 to 1 with increasing t.

Corresponding to such a time variation of charge, a current flows in the dielectric as shown in Figure. 2.6. The currents that flow instantaneously immediately after charging and

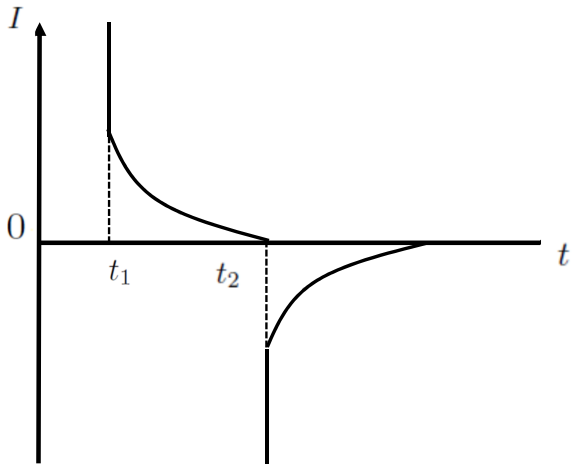

Figure 2.6: Time variation of current

discharging are called instantaneous charge current and instantaneous discharge current, respectively. The currents that decay with time in the charging or discharge process are called absorption currents. Let I_1 denote the instantaneous charging current and dV/dt denote the rate of voltage rise immediately after the voltage is applied at $t = t_1$, then

$$I_1 = C_1 \frac{dV}{dt} = \varepsilon_{r\infty} C_0 \frac{dV}{dt}. \tag{2.25}$$

Let $I_d(t)$ be the absorbed current, and let

$$I_d(t) = \frac{dQ_d(t)S}{dt} = (C_2 - C_1)\frac{df}{dt} \cdot V = (C_2 - C_1)\phi(t)V = (\varepsilon_{r0} - \varepsilon_{r\infty})C_0\phi(t)V \tag{2.26}$$

correspond to the (2.24) equation. Where $\phi(t) = df(t)/dt$. Therefore, the total current I during charging is

$$I = C_1\frac{dV}{dt} + (C_2 - C_1)\phi(t)V. \tag{2.27}$$

For linear dielectrics, the total current during discharge is equal to the expression (2.27) with only the sign changed.

$\phi(t)$ is a function that has the property of

$$\int_0^\infty \phi(t)dt = \int_0^\infty \frac{df}{dt} \cdot dt = 1 \tag{2.28}$$

as described in (2.24), and that decays with time to zero at the end. This is called the aftereffect function, which is a quantity that characterizes the relaxation phenomenon.

Next, we consider the relationship between time-varying voltage and current. A voltage that varies with time in the form of a staircase is applied to the capacitor as shown in Figure refstepdenatu. In this case, the absorbed current is the sum of all the absorbed currents

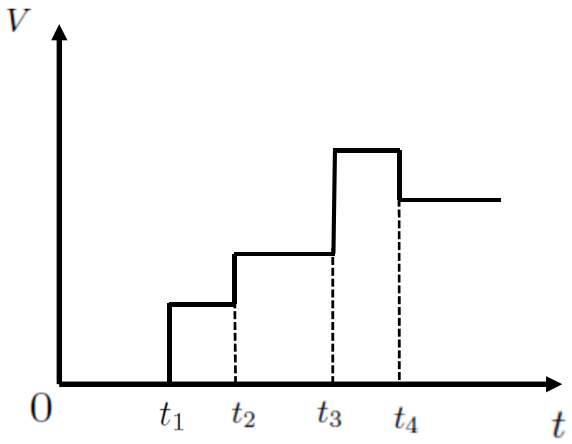

Figure 2.7: step voltage

that flow according to the voltages applied one after another, such as $\Delta V(t_1)$ at $t = t_1$ and $\Delta V(t_2)$ at $t = t_2$ as shown in Figure refstepdenatubunkai. Therefore, the absorbed current

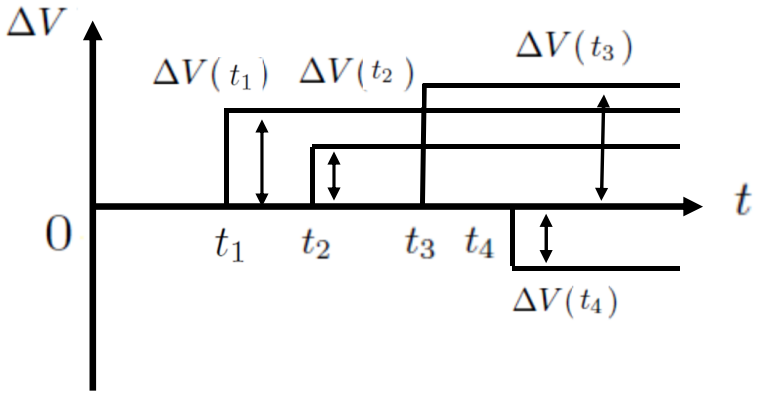

Figure 2.8: Decomposed step voltage

at a certain time $t(t > t_{\mathrm{i}})$ when a voltage such as figure.2.7 is applied can be written as

$$I_d(t) = (C_2 - C_1) \sum_{i=1}^{\mathrm{i}} \Delta V(t_{\mathrm{i}}) \phi(t - t_{\mathrm{i}}) \tag{2.29}$$

The fact that the absorbed current can be obtained by such a superposition method is called Hopkinson's superposition principle.

Furthermore, consider the case shich a voltage that varies continuously with time is applied. In this case, since it can be considered equivalent to applying minute voltages $dV(u)$ one after another at every infinitesimally small time interval du, we can rewrite the expression (2.29) in the integral form. Therefore, we have

$$I_{\mathrm{d}}(t) = (C_2 - C_1) \int_{-\infty}^{t} \frac{\mathrm{d}V(u)}{\mathrm{d}u} \phi(t - u) du. \tag{2.30}$$

Here, we set

$$t - u \equiv x, \tag{2.31}$$

The formula (2.30) eventually becomes

$$I_{\mathrm{d}}(t) = (C_2 - C_1) \int_{0}^{\infty} \frac{\mathrm{d}V(t - x)}{\mathrm{d}t} \phi(x) dx. \tag{2.32}$$

On the other hand, since the charging current corresponding to Eq. (2.25) exists over the all time range of the applied voltage, the total current I eventually becomes

$$I = C_1 \frac{\mathrm{d}V(T)}{\mathrm{d}t} + (C_2 - C_1) \int_{0}^{\infty} \frac{\mathrm{d}V(t - x)}{\mathrm{d}t} \phi(x) dx. \tag{2.33}$$

2.1.5 Relation between complex permittivity and response function

In equation (2.33), if $V(t)$ is the AC voltage $V(t) = V_0 e^{i\omega t}$, the total current is as follows

$$I = i\omega V\left\{(C_2 - C_1)\int_0^\infty e^{-i\omega x}\phi(x)dx\right\} \tag{2.34}$$

$$= i\omega V\left\{(C_2 - C_1)\int_0^\infty \phi(x)\cos(\omega x)dx\right\} + \omega V(C_2 - C_1)\int_0^\infty \phi(x)\sin(\omega x)dx. \tag{2.35}$$

Substituting equations (2.22) and (2.23) into equations (2.34) and (2.35), we obtain

$$I = i\omega C_0 V\left\{\varepsilon_{r\infty} + (\varepsilon_{r0} - \varepsilon_{r\infty})\int_0^\infty e^{-i\omega x}\phi(x)dx\right\} \tag{2.36}$$

$$= i\omega C_0 V\left\{\varepsilon_{r\infty} + (\varepsilon_{r0} - \varepsilon_{r\infty})\int_0^\infty \phi(x)\cos(\omega x)dx\right\} + \omega C_0 V(\varepsilon_{\mathrm{r}0} - \varepsilon_{r\infty})\int_0^\infty \phi(x)\sin(\omega x)dx. \tag{2.37}$$

On the other hand, since the relationship between the voltage and current of the dielectric capacitor in AC can also be expressed by the equation (2.19), the following relationship can be obtained by comparing with the equations (2.36) and (2.37).

$$\varepsilon^*_{\mathrm{r}}(\omega) = \varepsilon_{r\infty} + (\varepsilon_{\mathrm{r}0} - \varepsilon_{\mathrm{r}\infty})\int_0^\infty \phi(x)e^{-i\omega x}dx \tag{2.38}$$

or

$$\frac{\varepsilon'_r(\omega) - \varepsilon_{\mathrm{r}\infty}}{\varepsilon_{r0} - \varepsilon_{r\infty}} = \int_0^\infty \phi(x)\cos(\omega x)dx \tag{2.39}$$

$$\frac{\varepsilon''_r(\omega)}{\varepsilon_{\mathrm{r}0} - \varepsilon_{\mathrm{r}\infty}} = \int_0^\infty \phi(x)\sin(\omega x)dx \tag{2.40}$$

These equations express the relationship between the complex permittivity and the aftereffect function, and if the aftereffect function is known, the pattern of variation of the complex permittivity with frequency can be determined. Applying the Fourier transform to these equations yields the inverse relation

$$\phi(x) = \frac{2}{\pi}\int_0^\infty \frac{\varepsilon'_{\mathrm{r}}(\omega) - \varepsilon_{\mathrm{r}\infty}}{\varepsilon_{r0} - \varepsilon_{\mathrm{r}\infty}}\cos(\omega x)d\omega \tag{2.41}$$

$$\phi(x) = \frac{2}{\pi}\int_0^\infty \frac{\varepsilon''_{\mathrm{r}}(\omega)}{\varepsilon_{\mathrm{r}0} - \varepsilon_{\mathrm{r}\infty}}\sin(\omega x)d\omega \tag{2.42}$$

then, If the frequency variation of dielectric constant and dielectric loss are known, the pattern of time variation of the aftereffect function can be determined.

2.1.6 Principle of complex permittivity measurement

For measurement in the frequency range that can be treated as a concentrated constant circuit (approx. 100 MHz or lower), the equivalent parallel capacitance C and equivalent parallel conductance G of the sample are measured using a parallel plate capacitor, and the dielectric constant and relative dielectric constant are calculated from the equations (2.13) and (2.14). Although it is difficult to measure AC in the very low frequency region below 0.1Hz, the absorbed current $I_{\mathrm{d}}(t)$ under DC voltage can be measured and the dielectric constant and dielectric loss can be calculated based on the theory described in the previous sections. That is, if the capacitance of the electrode with a sample is C_0 and the applied voltage is V, the aftereffect function $\phi(t)$ is

$$\phi(t) = \frac{I_{\mathrm{d}}(t)}{(\varepsilon_{\mathrm{r}0} - \varepsilon_{\mathrm{r}\infty})C_0 V} \tag{2.43}$$

from the equation (2.26). Substituting this into equations (2.39) and (2.40) yields

$$\varepsilon'_{\mathrm{r}}(\omega) - \varepsilon_{\mathrm{r}\infty} = \frac{1}{C_0 V}\int_0^\infty I_{\mathrm{d}}(t)\cos(\omega t)dt \tag{2.44}$$

$$\varepsilon''_{\mathrm{r}}(\omega) = \frac{1}{C_0 V}\int_0^\infty I_{\mathrm{d}}(t)\sin(\omega t)dt \tag{2.45}$$

and $\varepsilon'_{\mathrm{r}}(\omega) - \varepsilon_{\mathrm{r}\infty}$ and $\varepsilon''_{\mathrm{r}}(\omega)$ are obtained from the absorbed current.

2.1.7 Debye's theory

In a polar liquid or solution, when no electric field acts, the dipole moments of individual polar molecules take disordered directions due to Brownian motion, and the whole solution shows no dipole moment. When an electric field acts, the force to rotate the polar molecules due to the frictional resistance between them and the surrounding molecules and the Brownian motion form a statistical equilibrium state and induce dipole moments in the direction of the electric field as a whole. Debye's theory deals with polarization phenomena under the action of time-varying electric field based on this idea. The complex permittivity $\varepsilon^*_{\mathrm{r}}$ at angular frequency ω is given by the following equation, called Debye's function

$$\varepsilon^*_{\mathrm{r}} = \varepsilon_{\mathrm{r}\infty} + \frac{\varepsilon_{\mathrm{r}0} - \varepsilon_{\mathrm{r}\infty}}{1 + i\omega\tau_0}. \tag{2.46}$$

Where, ε_{r0} and $\varepsilon_{r\infty}$ are the dielectric constants at very low (ε_{r0}) and high ($\varepsilon_{r\infty}$) frequencies compared to ε_{r0} and $\varepsilon_{r\infty}$, respectively, τ_0 is

$$\tau_0 = \frac{\varepsilon_{r0} + 2}{\varepsilon_{r\infty} + 2}\tau. \tag{2.47}$$

Where τ is the relaxation time, which can be regarded as the time required for the rotation of the dipole. Let ζ be the magnitude of the frictional resistance of the dipole to the surrounding molecules during its rotation, k be Boltzmann's constant, and T be the absolute temperature, then

$$\tau = \frac{\zeta}{2kT}. \tag{2.48}$$

If a molecule forming a dipole is regarded as a rigid sphere of radius a and rotates at a constant angular velocity in a medium of viscosity eta, the relaxation time is given by

$$\zeta = 8\pi a^3 \eta \tag{2.49}$$

and

$$\tau = \frac{8\pi a^3 \eta}{2kT} \tag{2.50}$$

by Stokes' law, and the relaxation time is proportional to the viscosity.

Decomposing both sides of the equation (2.46) into real and imaginary parts and rearranging them, we obtain the following expressions for the frequency dependence of dielectric permittivity and dielectric loss.

$$\varepsilon'_r = \varepsilon_{r\infty} + \frac{\varepsilon_{r0} - \varepsilon_{r\infty}}{1 + \omega^2 \tau_o^2} \tag{2.51}$$

$$\varepsilon''_r = \frac{(\varepsilon_{r0} - \varepsilon_{r\infty})\omega\tau_0}{1 + \omega^2 \tau_o^2} \tag{2.52}$$

Also, using the relationship in equation (2.18), $\tan\delta$ becomes

$$\tan\delta = \frac{(\varepsilon_{r0} - \varepsilon_{r\infty})\omega\tau_0}{\varepsilon_{r0} + \varepsilon_{r\infty}\omega^2\tau_0^2}. \tag{2.53}$$

2.1.8 Relaxation functions

Experimentally, obtaind data by dielectric measurements often show deviation from the Debye function. Several empirical formulas for describing such data will help us to analyze

them. Namely, Cole-Cole (CC) function [30]:

$$\varepsilon^* = \frac{\Delta\varepsilon}{1 + (i\omega\tau)^{\delta}}, \tag{2.54}$$

Davidson-Cole (DC) function [31]:

$$\varepsilon^* = \frac{\Delta\varepsilon}{(1 + (i\omega\tau)^{\delta})^{\gamma}}. \tag{2.55}$$

and Havriliak-Negami (HN) function [32]:

$$\varepsilon^* = \frac{\Delta\varepsilon}{(1 + (i\omega\tau)^{\delta})^{\gamma}}. \tag{2.56}$$

The exponents δ and γ take values in the range of $0 < \delta \leq 1$ and $0 < \gamma \leq 1$. Since they represent symmetric or asymmetric deviations from the Debye-type dielectric dispersion, they are called symmetric and asymmetric parameters, respectively. HN formula is the most general form and is consistent with the DC formula if $\gamma \neq 1, \delta = 1$, the CC formula if $\gamma = 1, \delta \neq 1$, and the Debye formula if $\gamma = 1, \delta = 1$. The frequency dependences of the complex permittivity of some empirical equations are shown in figure 2.9.

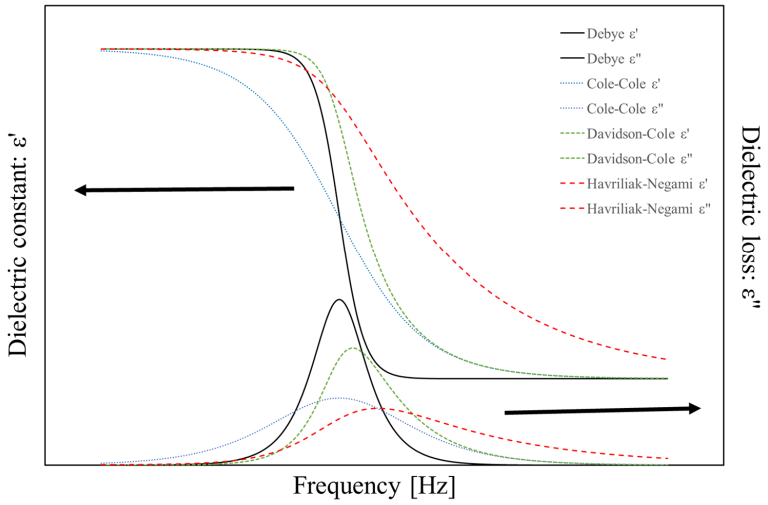

Figure 2.9: Example of relaxation functions. Debye: $\gamma = 1, \delta = 1$, CC: $\gamma = 1, \delta = 0.5$, DC: $\gamma = 0.5, \delta = 1$, HN: $\gamma = 0.3, \delta = 0.7$.

2.2 Broadband dielectric spectroscopy

Since the dielectric dispersion of glass-forming materials is observed over a wide range of frequencies, we performed measurements over a wide frequency range by combining several devices such as Figure 2.10.

In this study, we apply this method, so-called Broadband Dielectric Spectroscopy (BDS)

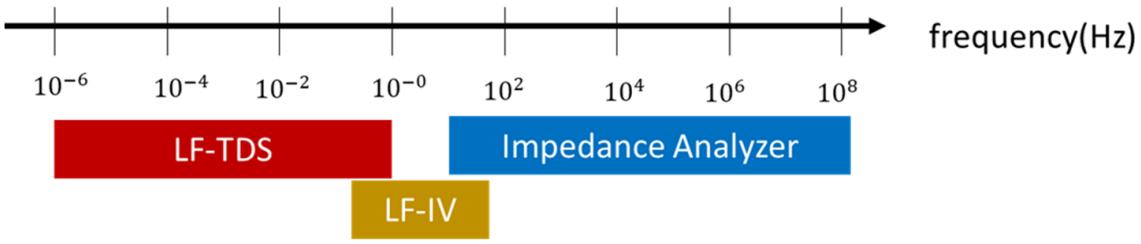

Figure 2.10: Frequency range covered by each experimental technique.

from 10μHz to 110MHz.

2.2.1 LF-TDS

It can be measured from 10^{-6} to 10^{-1}[Hz]. In this frequency region, α relaxation near the glass transition temperature is observed, so that this is the most important method in this study. The devices were connected as shown in figure 2.11. DC voltage of 10 V was applied for 0.8 s with an A/D converter (MCI Engineering DAM-702GPC). The charge and discharge currents were measured with an oscilloscope (Tektronix TDS210) and an amperometer (Keithley 6512).

In the low frequency range, parallel plate dielectric cell(see Figure 2.12) is used. This capacitor has a diameter of 50 mm and the standard capacitance of 174 pF. The capacitor is charged for a time corresponding to the measurement frequency and then discharged for the same time. Although both charging and discharging currents can be measured, the discharging current is used for the analysis phase because the charging current includes DC conductivity. For example, the discharge current after charging grycerol at 193K for 10^5

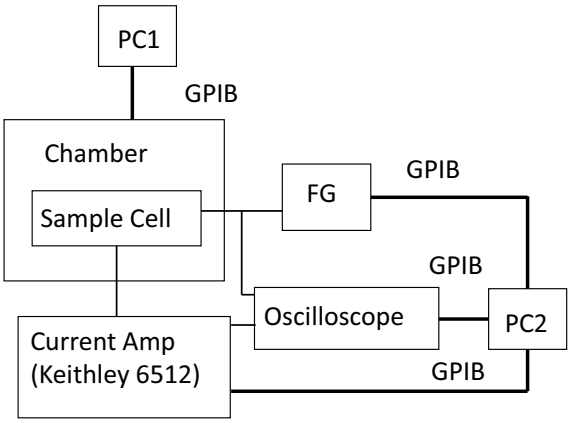

Figure 2.11: System block of LF-TDS

seconds is as shown in Figure 2.13.

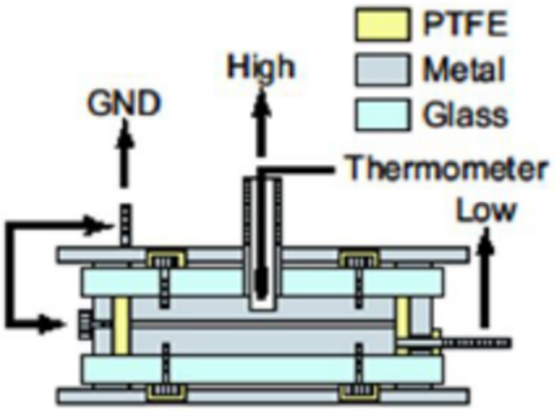

Figure 2.12: Dielectric cell for low-frequency range.

The complex permittivity is calculated as

$$\varepsilon^*(\omega) = \frac{\mathscr{F}i}{i\omega C_0 \mathscr{F}v} \tag{2.57}$$

using $\mathscr{F}i$ and $\mathscr{F}v$, which are Fourier transforms of the current i and voltage v obtained in this way, respectively.

As a result, we obtain complex permittivities in the range shown in Figure 2.14.

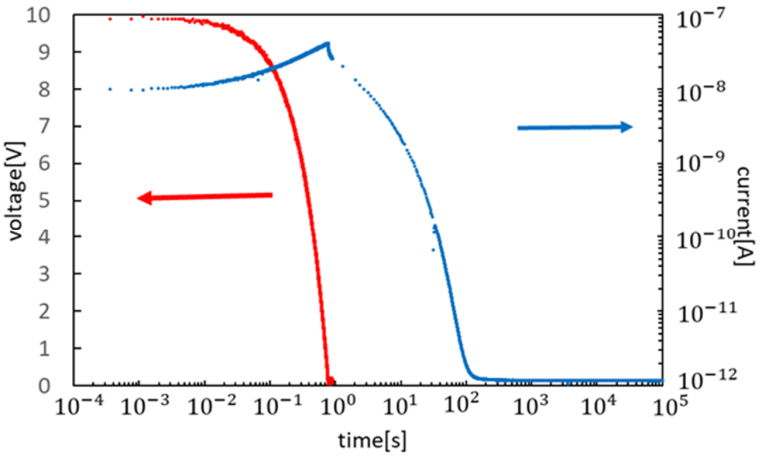

Figure 2.13: Example of applyed voltage and discharging current. The sample is grycerol at 193 K.

2.2.2 LF-IV

It can measure from 10^{-1} to 80[Hz]. Each device was connected as shown in figure 2.15, AC voltage was applied using a function generator (Yokogawa FG110), and the response current was measured using an oscilloscope (model number) and a current amplifier (Keithley 428). In this measurement method, the same sample cell as the LF-TDS is used. The obtained current $\boldsymbol{I}$ and voltage $\boldsymbol{V}$ are used to calculate the complex permittivity as

$$\varepsilon^*(\omega) = \frac{\boldsymbol{I}}{i\omega C_0 \boldsymbol{V}}. \tag{2.58}$$

As a result, we obtain complex permittivities in the range shown in Figure 2.16.

2.2.3 Impedance analyzer

The complex admittance can be measured from 40Hz to 110MHz using an impedance analyzer (Keysight 4294A). And calculate the complex permittivity using the formula (2.59).

$$Z = \frac{1}{i\omega C_0 \varepsilon^*(\omega)} \tag{2.59}$$

Sample cell is used OPPC(Outward Parallel Plate Cell) cell [33] developed by us. The capacitor with a diameter of 50 mm and an inner diameter of 7 mm with a hole in the center and the standard capacitance of 170 pF.

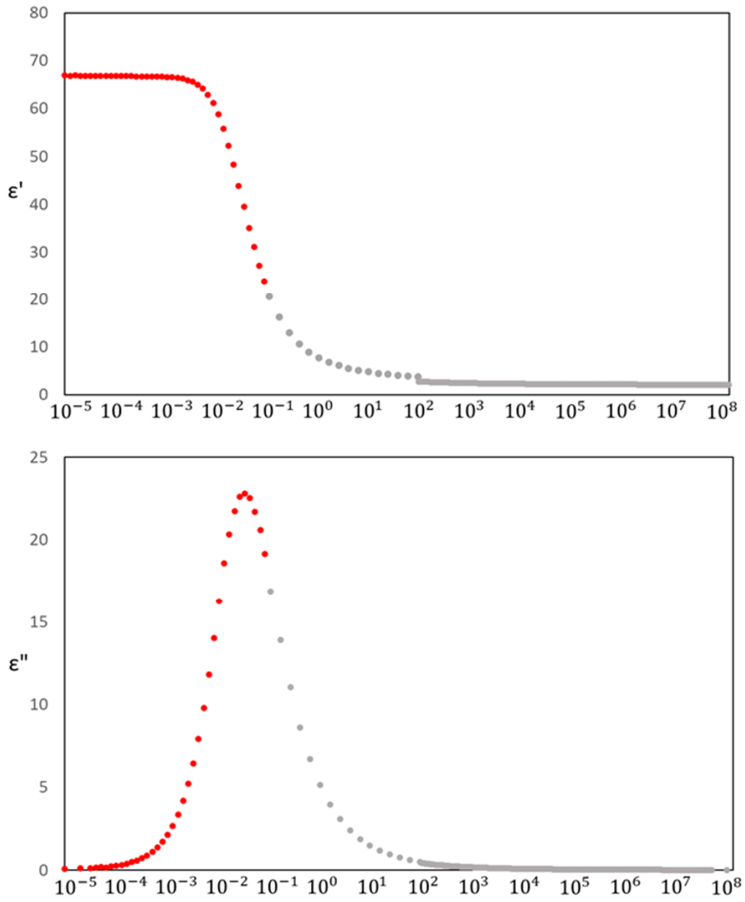

Figure 2.14: Frequency range for the LF-TDS. The red area is the corresponding frequency range.

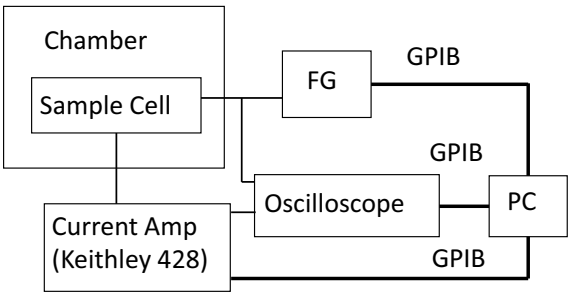

Figure 2.15: System block of LF-IV

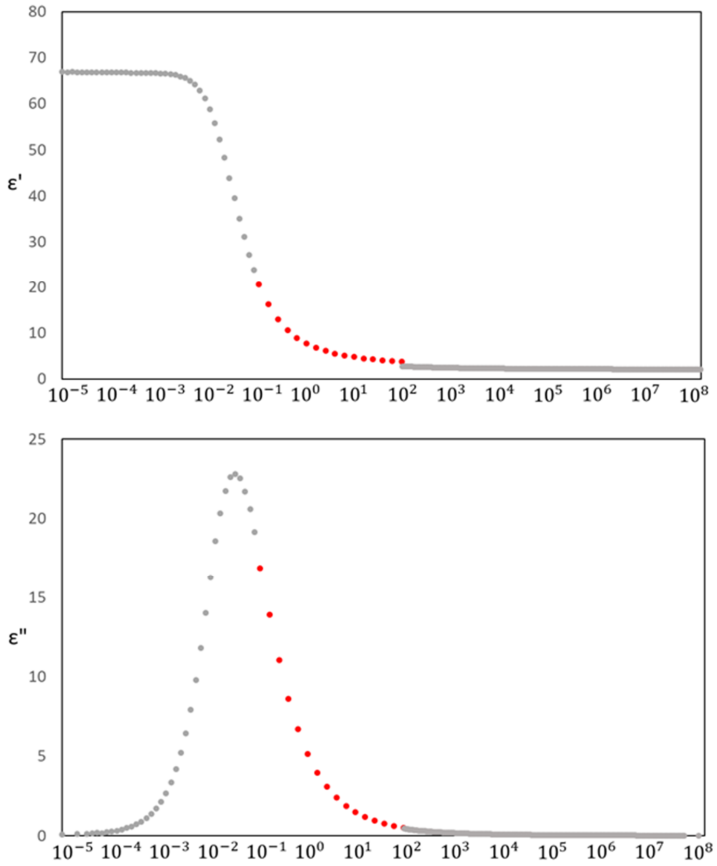

Figure 2.16: Frequency range for the LF-IV. The red area is the corresponding frequency range.

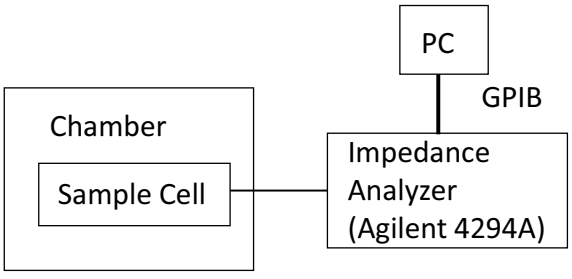

Figure 2.17: System block of Impetance Analyzer

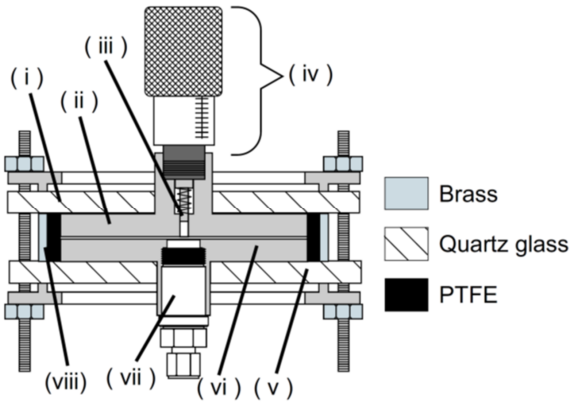

Figure 2.18: Dielectric cell for Impetance Analyzer [33]. (i) upper supporting plate, (ii) upper electrode, (III) movable center pin, (iv) micrometer head, (v) lower supporting plate, (vi) lower electrode, (vii) APC7 connector, (viii) spacer.

As a result, we obtain complex permittivities in the range shown in Figure 2.19.

2.3 Samples

The sample of sorbitol ($CH_2OH(CHOH)_4CH_2OH$) and glycerol ($CH_2OH(CHOH)CH_2OH$) was purchased from Kishida Chemical and xylitol ($CH_2OH(CHOH)_3CH_2OH$) was purchased from Acros Organics. Before loading the samples into the dielectric cell, each sample were placed in a vacuum chamber at 308 K for more than 12 hours to remove adsorbed moisture. The loaded sample was annealed at a temperature above the melting points. Temperature of the dielectric cell was set to be the one below T_g for time period more than 28 hours. All the measurement procedure were proceeded during heating process. Dielectric measurements were performed at constant temperatures with pre-measurement waiting time period more than 10 times of the expected dielectric relaxation time of the sample being measured during heating process.

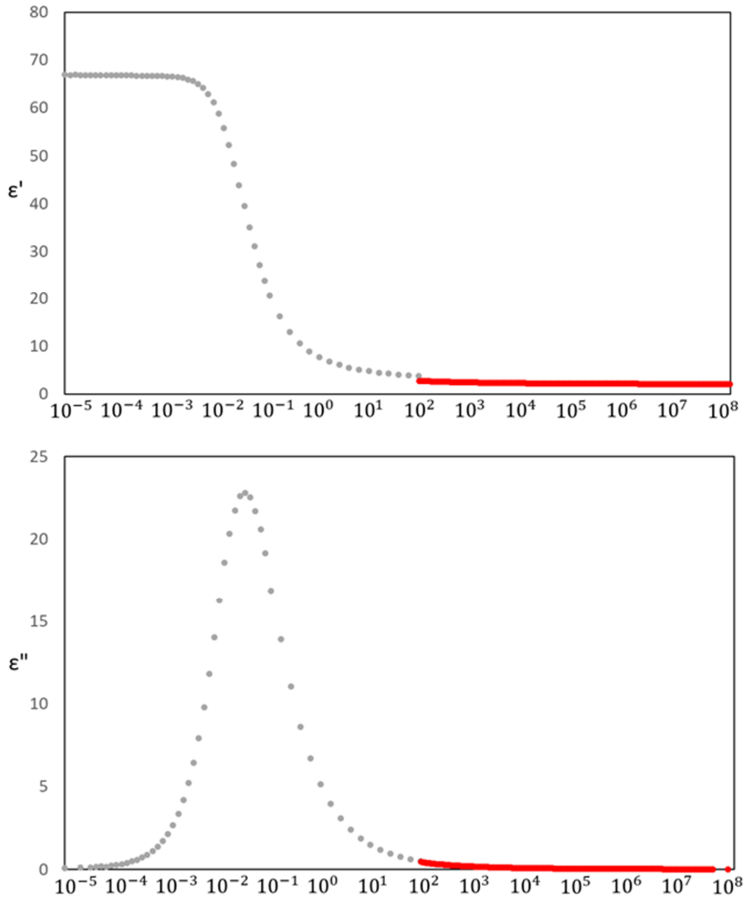

Figure 2.19: Frequency range for the Impedance Analyzer. The red area is the corresponding frequency range.

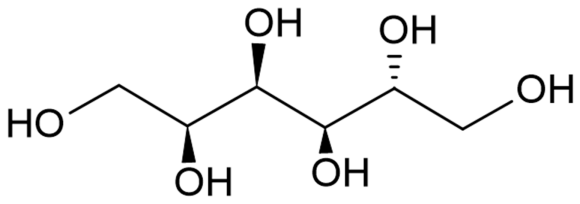

Figure 2.20: Structural formula of sorbitol.

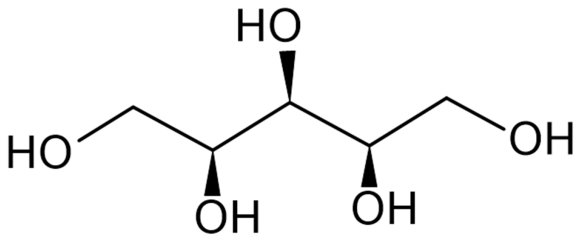

Figure 2.21: Structural formula of xylitol.

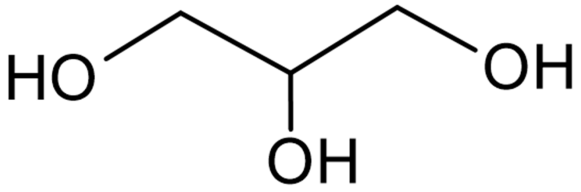

Figure 2.22: Structural formula of grycerol.

2.4 Evaluation of dielectric dispersion

All the dispersion data of complex permittivity in this study show one or two dielectric relaxation process corresponding to the α and JG-β processes. Therefore, we analyzed the dispersions using a superposition of two Havriliak-Negami (HN) equations [32], that is,

$$\varepsilon^* = \varepsilon_\infty + \frac{\Delta\varepsilon^\alpha}{(1+(i\omega\tau_{\mathrm{HN}}^\alpha)^{\delta^\alpha})^{\gamma^\alpha}} + \frac{\Delta\varepsilon^\beta}{1+(i\omega\tau_{\mathrm{CC}}^\beta)^{\delta^\beta}} \tag{2.60}$$

where, $\varepsilon^* = \varepsilon' - i\varepsilon$" is the complex permittivity with the dielectric loss, $\Delta\varepsilon$ is the dielectric strength, τ is the dielectric relaxation time, ω is the angular frequency, δ and γ are symmetric and non-symmetric parameters and ε_∞ is the high-frequency limiting permittivity. Super-suffix α and β correspond to the α and the JG-β processes. Finally, it was found that the α process can be well described by using the HN function and the JG-β process by the Cole-Cole (CC) function [30] (HN function with $\gamma = 1$). An example of the fitting is shown in figure 2.23.

Values of the α relaxation frequency (f_{m}^α) were given as a frequency with the maximum dielectric loss of the HN loss curve. f_{m}^α is calculated by following equation [34].

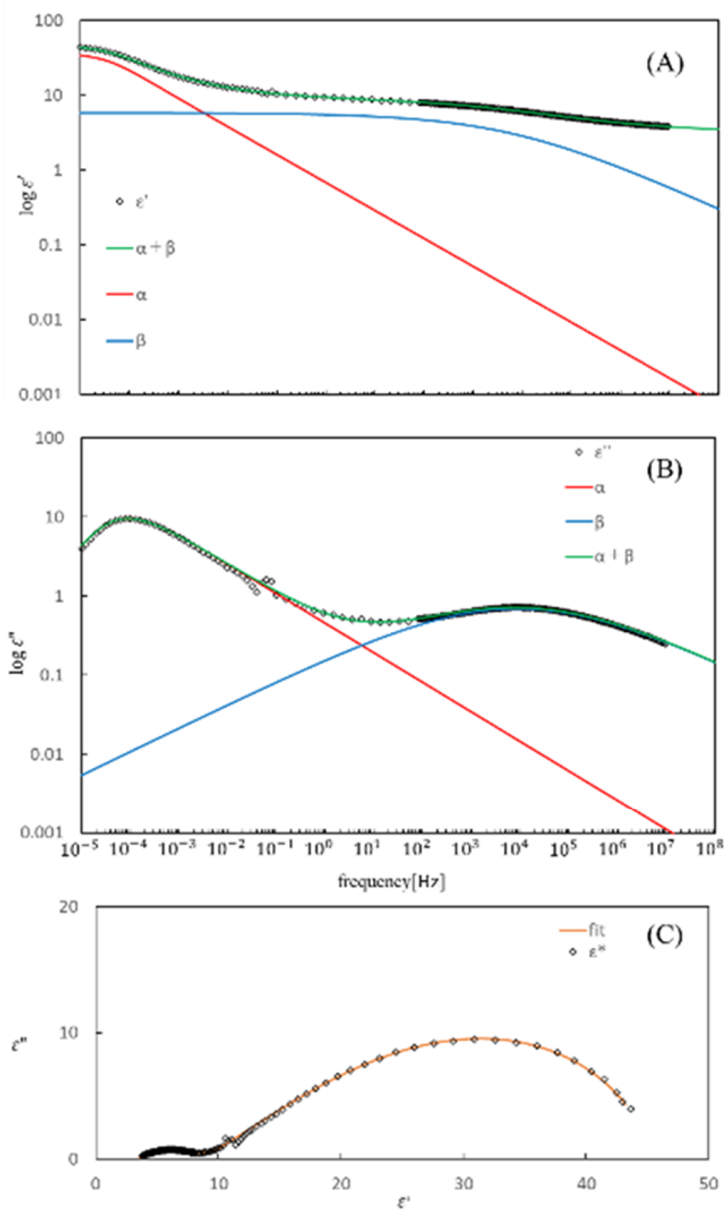

Figure 2.23: Dielectric constant (A) and loss (B) of sorbitol at 265 K (after 1075 hours annealing at this temperature). (C) Corresponding Cole-Cole plot. Plots are experimental data and the curves are given by equation (1).

$$f_{\mathrm{m}}^{\alpha} = \frac{1}{2\pi\tau_{\mathrm{HN}}^{\alpha}}\left[\tan\left(\frac{\pi}{2(\gamma^{\alpha}+1)}\right)\right]^{\frac{1}{\delta^{\alpha}}} \tag{2.61}$$

Chapter 3

Cell condition

3.1 Cell condition

First, we examined effect of dielectric cells with different mechanical features. We prepared two types of sample cells: one has fixed electrode gap (rigid-gap cell) and the other has movable gap which can change the gap with sample volume (movable-gap cell). The former is the parallel plate capacitor shown in figure 2.12 in the previous section, with the electrode spacing fixed at 100 μm by a brass ring. In the latter, Teflon sheets were used as spacers instead of brass rings as shown in figure 3.1. The spacers are squares 3 mm on a side and have initial thickness is 100 μm. Four spacers are placed to be rotationally symmetrical.

We used these cells to perform dielectric spectroscopy experiments with sorbitol at 265 K,

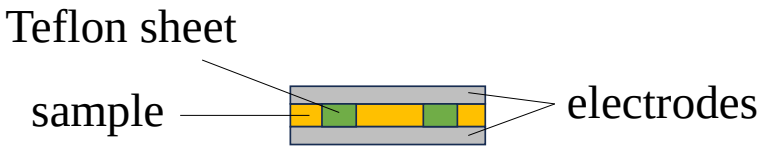

Figure 3.1: Schematic picture of the movable-gap cell.

near the glass transition temperature.

The frequency dependence of the dielectric loss obtained with each cell is shown in figure 3.2. Figure 3.3 shows the α relaxation frequencies f_m^α given by different cell conditions. The value of f_m^α by the movable-gap cell slightly larger than that by rigid-gal cell. On the other hand,

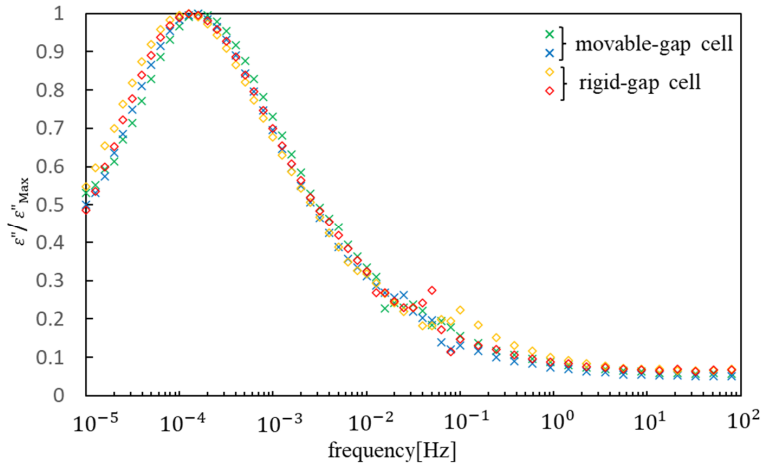

Figure 3.2: Normalized complex permittivity for sorbitol at 265 K. The rigid-gap cell is indicated by diamonds and movable-gap cell is indicated by crosses. Note that the maximum dielectric losses are normalized because the gap of electrodes varies in use of movable-gap cells. Samples were cooled at 0.7 K. from above the melting point to below 265 K and we waited more than 28 hours before starting our measurements.

it is also found that all data of this study have clearly smaller f_{m}^{α} than that of our previous study at 265 K with a rigid-gap cell.

Qualitatively, the movable-gap cell is expected to increase the sample density with decreasing temperature and decrease the relaxation frequency. From Figure 3.3, contrary to our expectation, the relaxation frequencies for the movable-gap cell are larger than that for the rigid-gap cell. It has been reported that the α relaxation frequency is quite sensitive to water content. This may cause such unexpected result. From Figure 3.3, compared to our previous study, the relaxation frequencies for both cells were small. As is discussed below, it is considered that the sample obtained in our previous study was not well relaxed at the lower temperatures including near T_{g}. Therefore, these results suggest that the effect of the cell condition on the relaxation frequency is very small compared to that due to the thermal history.

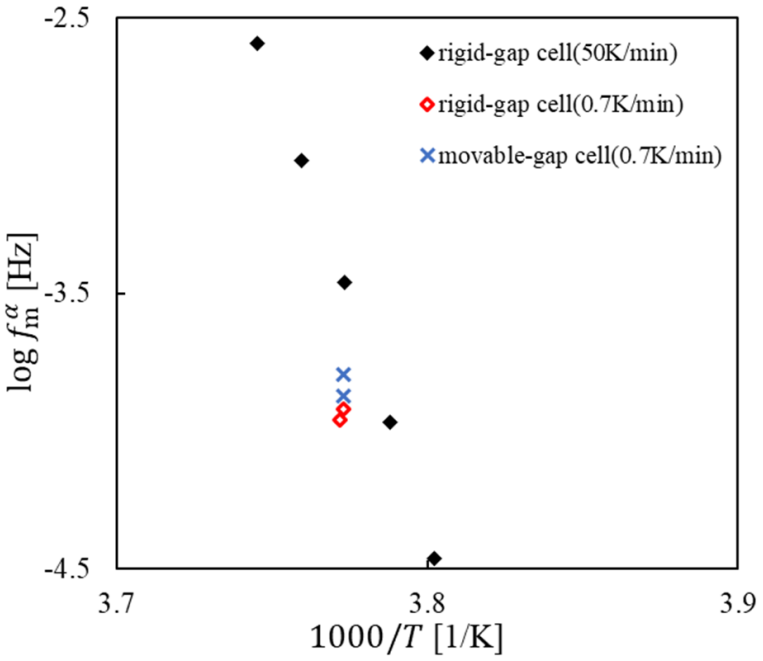

Figure 3.3: Plots of $\log f_{\mathrm{m}}^{\alpha}$ of sorbitol against $1000/T$. Open diamonds and cross markers indicate data with 0.7 K. cooling using rigid-gap cell and soft-gap cell respectively. Solid diamonds indicate data with about 50 K/min. cooling taken from the previous study [11]

Chapter 4

Effect of the thermal history

4.1 Effect of the thermal history

We prepared supercooled sorbitol, xylitol and glycerol as samples as is described in Method section. T_0 investigate the change in relaxation frequency with cooling rate, two samples with different cooling rates were prepared for each material. We classify dielectric measurements of samples into group-A and group-B according to cooling rate in decreasing temperature before starting measurement procedure. The cooling rate of group-A glycerol, xylitol and sorbitol is 0.7 K/min. and the measured temperature range are 193 K to 273 K, 267 K to 293 K and 265 K to 343 K respectively. The cooling rate of group-B glycerol is 3.8 K/min. and group-B sorbitol is 7.2 K/min. For the group-B, the measurement temperature is 193 K and 265 K to 295 K respectively. For group-A sorbitol, measurements were performed five times at 265 K with pre-measurement waiting time of 142 h, 379 h, 816 h, 1075 h and 1585 h. All these measurements were performed by using the rigid-gap cell.
We obtained frequency dependence of the complex permittivity for each sample at different temperatures corresponding to supercooled liquid and they are shown in Figure 4.14.24.34.44.5. For xylitol, only group-A data between 267 K and 293 K were available due to the crystallization. Group-B glycerol was measured only at 193 K which is the lower limit of this experimental system.

As explained in the previous part, we performed fitting on the data and were able to represent all of them well with the superposition of the HN and CC formulas. Continuously,

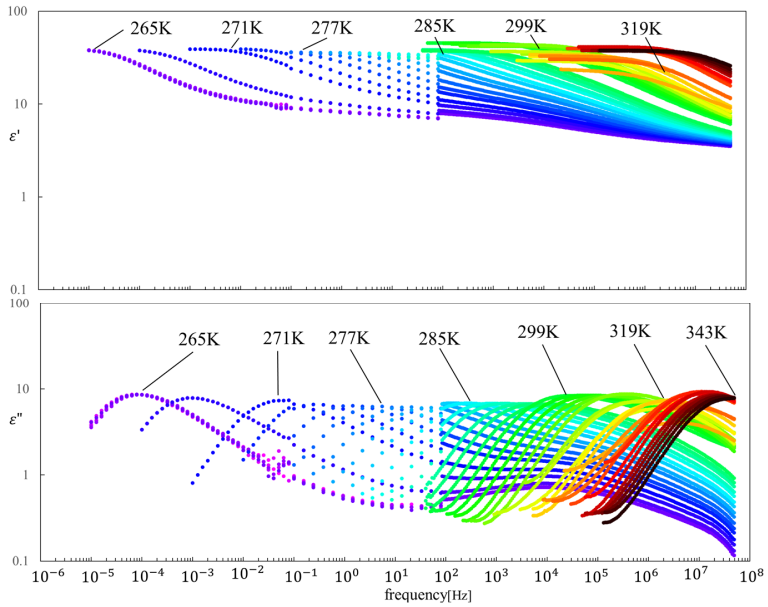

Figure 4.1: Dielectric constant and loss of group-A sorbitol. Samples were cooled at 0.7 K/min. from above the melting point to below 265 K and we waited more than 142 hours before starting our measurements.

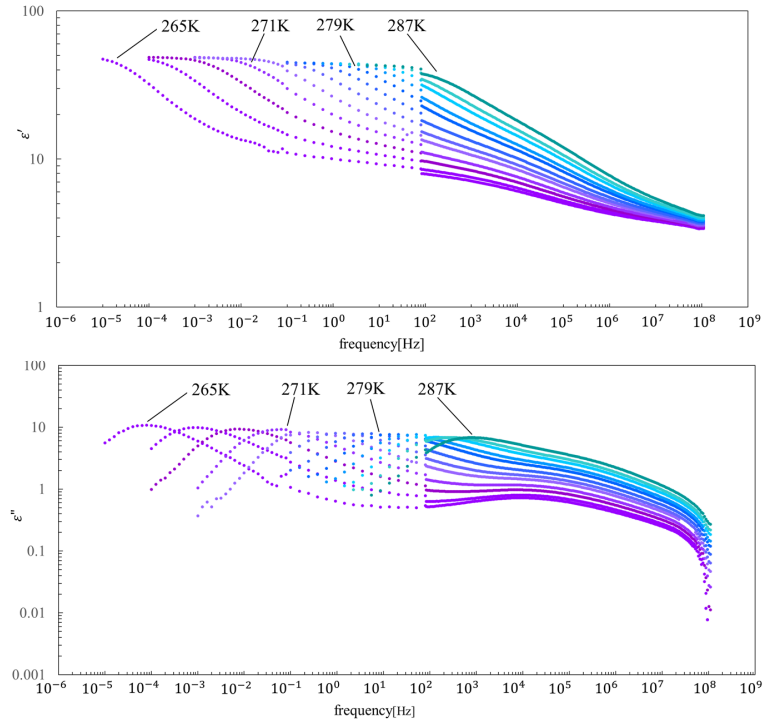

Figure 4.2: Complex permittivity for group-B sorbitol

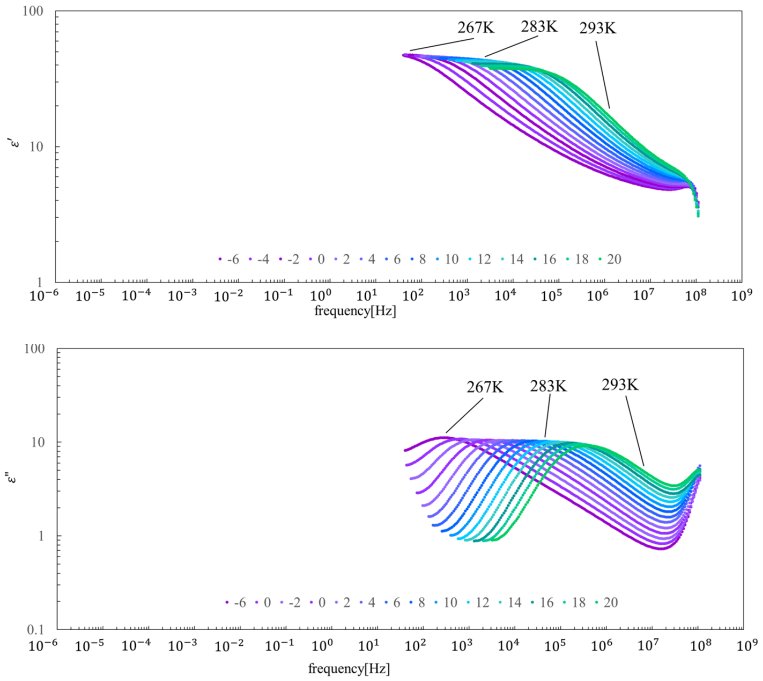

Figure 4.3: Complex permittivity for group-A xylitol

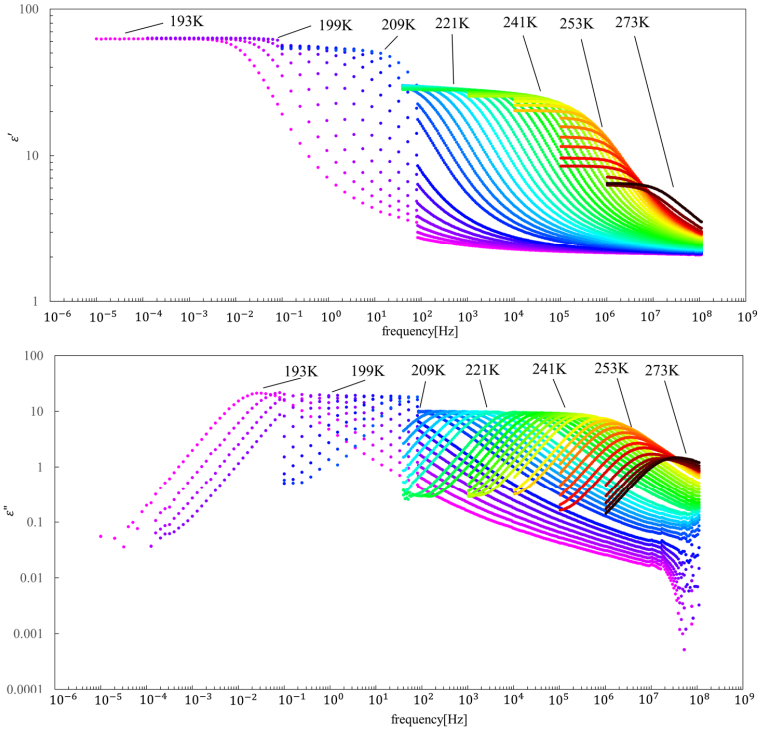

Figure 4.4: Complex permittivity for group-A grycerol

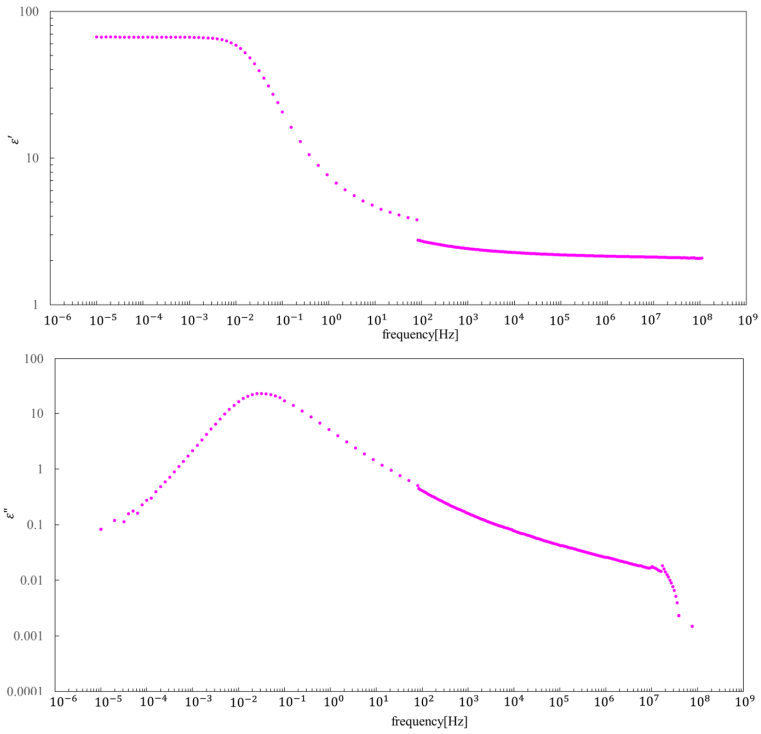

Figure 4.5: Complex permittivity for group-B grycerol

we obtained the temperature dependence of the HN and CC parameters: $\Delta\varepsilon, \delta, \gamma$ and the α relaxation frequency: f_{m}^{α}.

The Arrhenius diagram is shown in Figure 4.6. Note that, we were able to obtain only 267 K to 293 K data for group-A xylitol due to the difficulty of avoiding crystallization when we set the cooling rate to 0.7 K/min. The Arrhenius diagram is shown in Figure 4.6. For all samples, the data show the VFT-like behavior and consist with previous studies [11, 35] at high temperature region well above T_{g}. However, compared to the previous studies, the data in this study tend to have smaller relaxation frequency at low temperature region near the glass transition temperature. We consider that this difference comes from the difference of thermal history.

Focusing on the differences between group-A and B to consider the cooling rate, both groups show similar temperature dependence. However, compared to the data from the previous study with rapid cooling (estimated to be 50 K/min), the data obtained in this

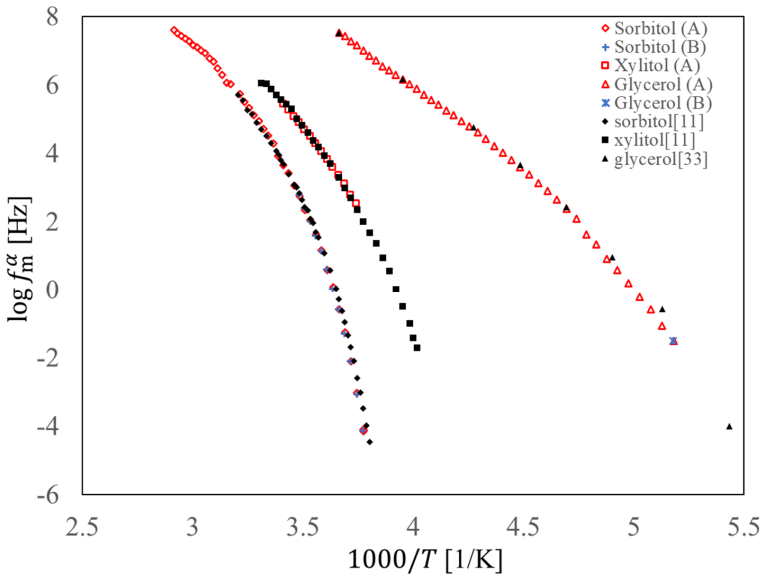

Figure 4.6: Relaxation map for glycerol and sorbitol at different cooling rates. Open triangles, squares and diamonds show group-A glycerol, xylitol and sorbitol with K/min.. cooling respectively. Asterisk and plus symbols show group-B glycerol and sorbitol with 3.8 K/min.. and 7.2 K/min. cooling respectively. Solid diamonds, squares and triangles are referred data of sorbitol [11], xylitol [11] and glycerol [35] respectively.

study clearly show a smaller relaxation frequency. The volume relaxation experiments on polymers [25] suggested that smaller cooling rates result in lower glass transition temperatures, and longer waiting times below the glass transition temperature bring the specific volume closer to the extrapolated line of quasi-equilibrium. It is natural that such differences in cooling rates and thermal history seems to have also affected to the dielectric relaxation frequency of the sugar alcohols.

Temperature dependence of dielectric parameters of HN and CC functions are indicated in Figure 4.7, 4.8 and 4.9. For the group-A sorbitol data, a discontinuity in the strength of α relaxation was observed. This would be caused by different sample preparation due to crystallization. The other parameters vary continuously with temperature. Although the measurement error or the analysis error may be included, there are few anomalies even in the region of T_g^*. Here, T_g^* is determined as the temperature at which f_{m}^{α}=0.01. It is considered that all the samples show no drastic change in nature in the temperature range of this study.

We tried to evaluate the temperature dependence of f_m^{α} of sorbitol using VFT equation. Figure 4.10 and 4.11 shows α relaxation frequency of group-A sorbitol and corresponding line given by the fitting procedure. In figure 4.11, to linearize the VFT expression, the horizontal axis is set to be $1/(T - T_0)$ with $T_0 = 234$K. It is clear that entire data of f_{m}^{α} is difficult to be well described by using a single VFT equation. Figure 4.12 shows the result of fitting with two VFT equations. They are considered to reproduce the data well. In other words, in sorbitol, the α process cannot be described by a single function over the entire temperature range, including just above the glass transition temperature.

Therefore, we have tried to determine the VFT equation for sorbitol using data above 273K. In this case, the data on the high temperature region are well described by the VFT equation. Finally, we found that f_{m}^{α} plots of sorbitol deviate from the VFT equation at temperatures lower than 269 K including near T_{g}

Figure 4.13 shows final results of $1/(T - T_0)$ analysis for f_{m}^{α}. Under the present conditions, glycerol and xylitol could be well represented by a single VFT function. On the other hand, values of f_{m}^{α} for sorbitol near T_g are deviate from the VFT equation determined using the higher temperatures. This suggests that the temperature dependence of f_{m}^{α} of sorbitol in the

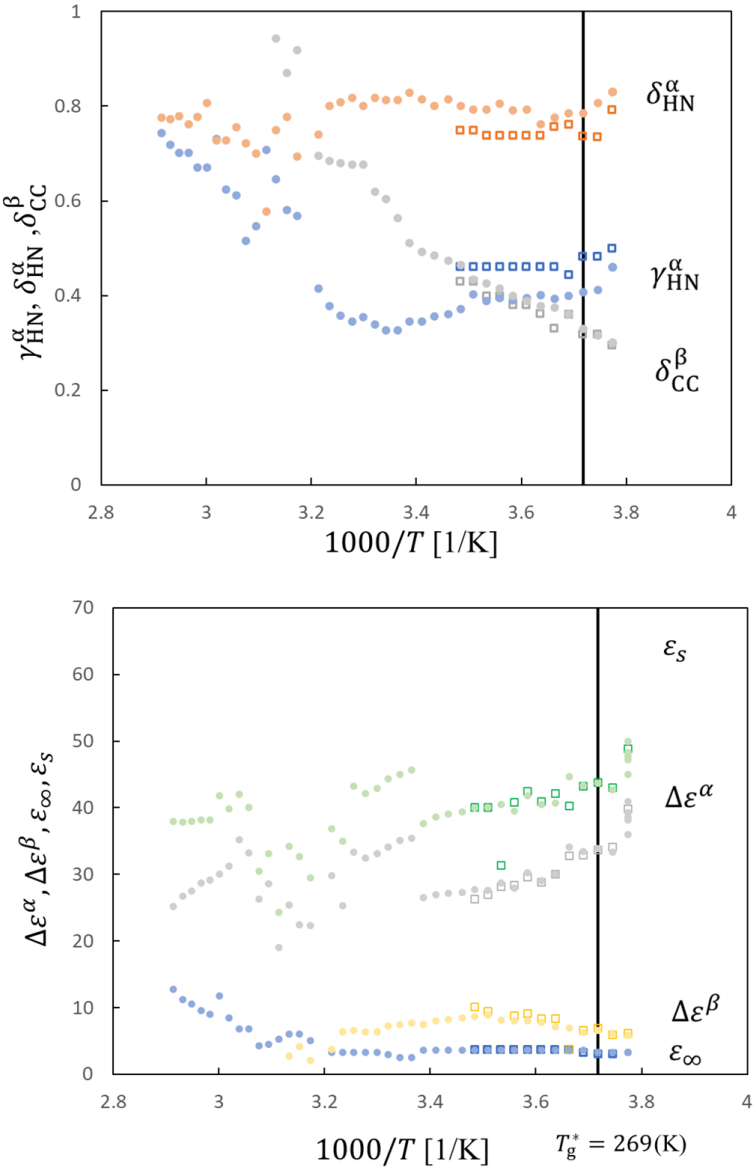

Figure 4.7: Fitting parameters of sorbitol. Solid circles indicate data with 0.7 K/min. cooling. Open squares indicate data with 7.2 K/min. cooling. The dashed line is drawn as a guide for the eye.

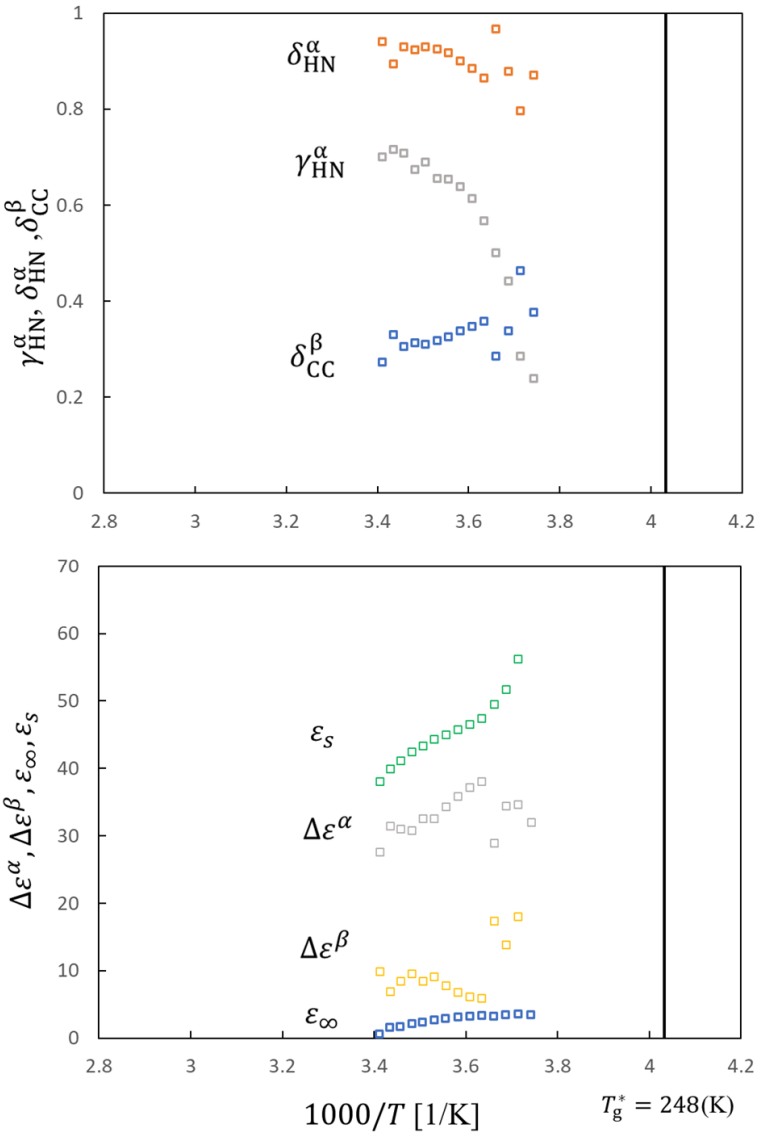

Figure 4.8: HN and CC parameters for xylitol. Open squares indicate data with 0.7 K/min. cooling.

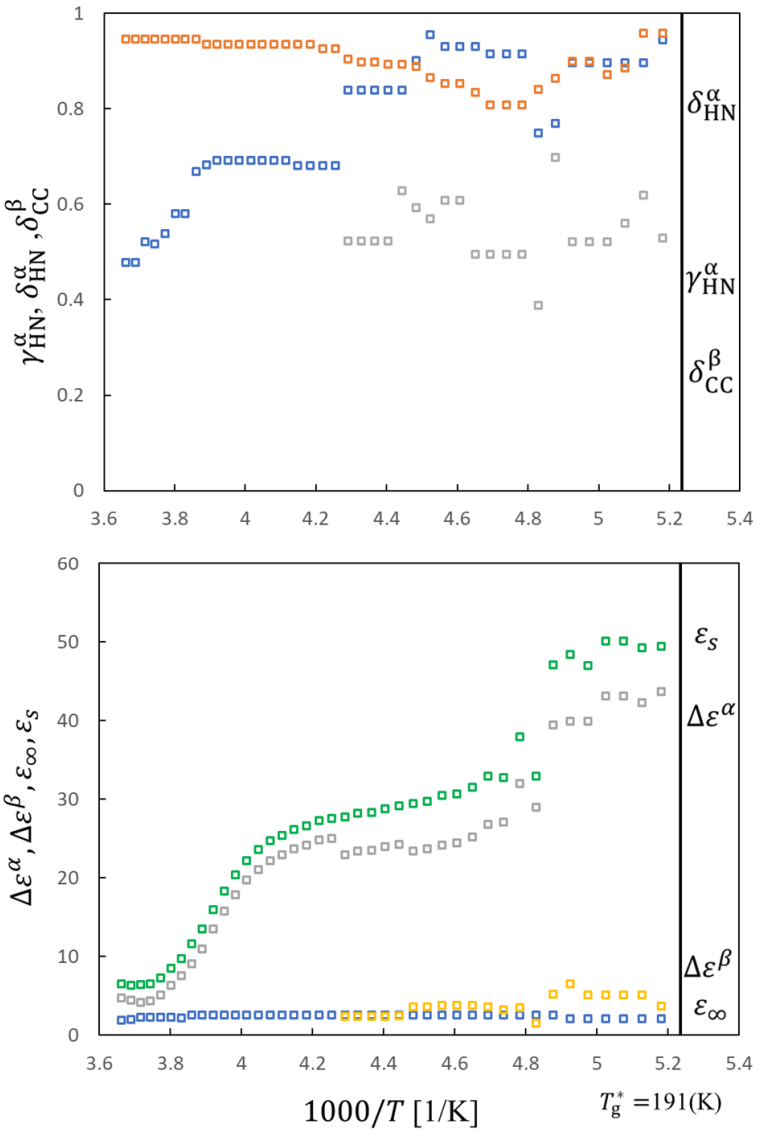

Figure 4.9: HN and CC parameters for grycerol. Open squares indicate data with 0.7 K/min. cooling.

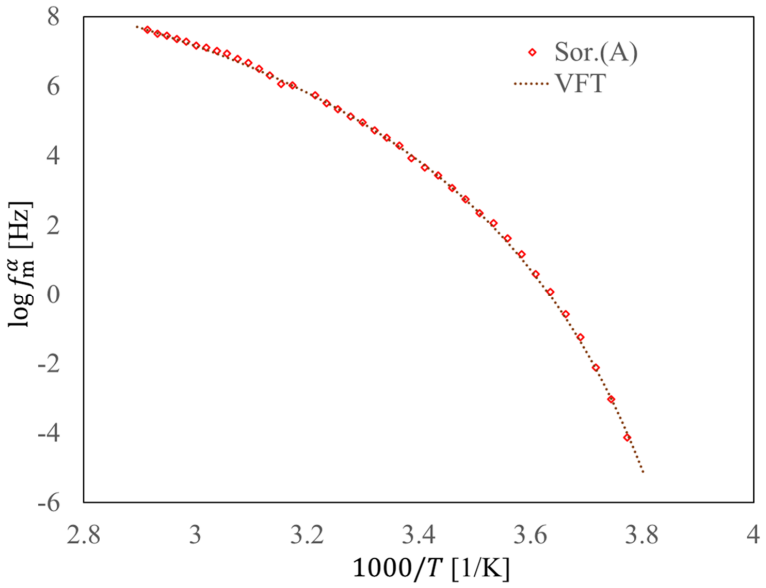

Figure 4.10: Arrhenius plot for solbitol. Fitting for group-A sorbitol with single VFT with $A = 12.2, B = 502$ and $T_0 = 234$.

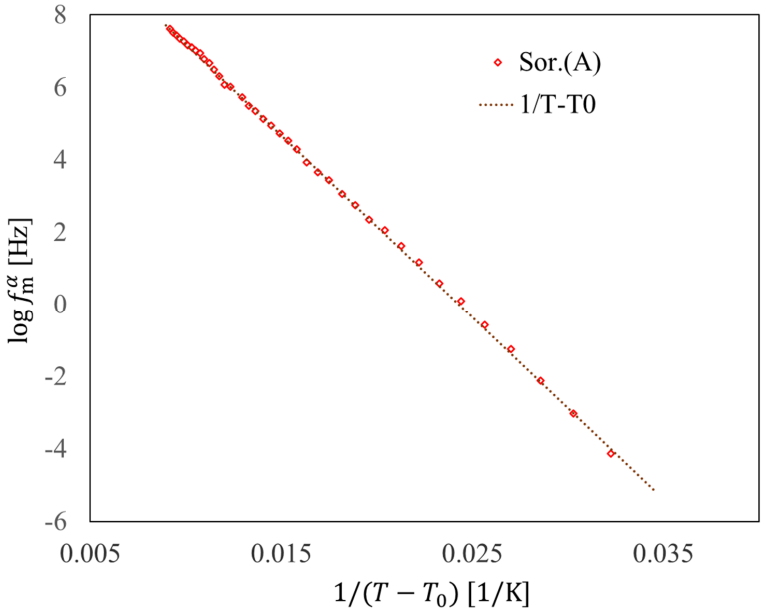

Figure 4.11: T-T0 for solbitol. Fitting for group-A sorbitol with single VFT. $T_0 = 234$.

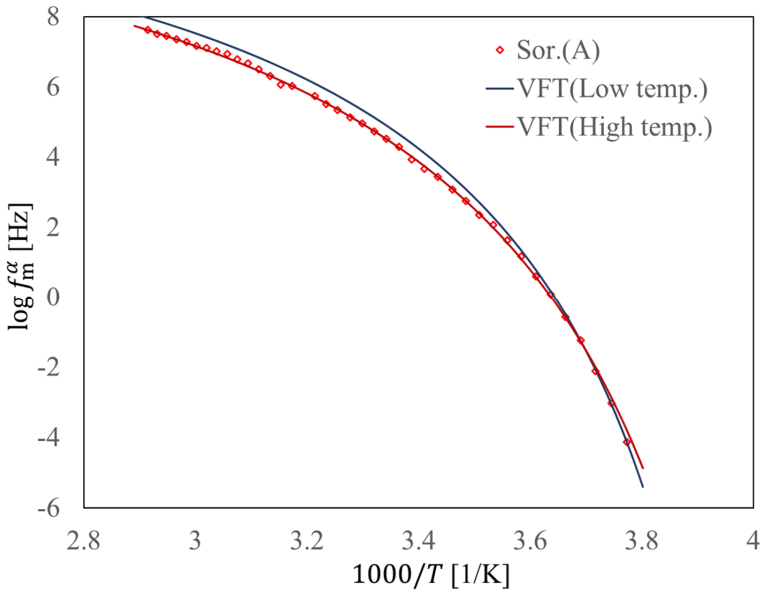

Figure 4.12: Arrhenius plot for solbitol. VFT fitting for group-A sorbitol with $A = 12.3, B = 515$ and $T_0 = 233$ for high temperature side and $A = 12.3, B = 460$ and $T_0 = 237$ for low temperature side.

entire temperature range investigated in this study is not represented only by using single VFT equation even if the sample is well relaxed to the sub-equilibrium state.

Experimental VFT parameters for all the samples are indicated in table 4.1. The VFT parameters obtained in this study change systematically with their characteristic quantities such as the carbon number N_C (3, 5 and 6 for glycerol, xylitol and sorbitol respectively) or T_g^* (192 K, 248 K and 269 K for glycerol, xylitol and sorbitol respectively). These results are considered to be very reasonable from the point of material natures.

Table 4.1: VFT parameters and characteristic quantities. A, B and T_0 are VFT parameters, N_C is carbon number and T_g^* is glass transition temperature which is determined by $f_m^\alpha = 0.01$.

sample	A	B	T_0	N_C	T_g^*
glycerol	14.0	939	133	3	192
xylitol	12.4	617	205	5	248
sorbitol	12.3	515	233	6	269

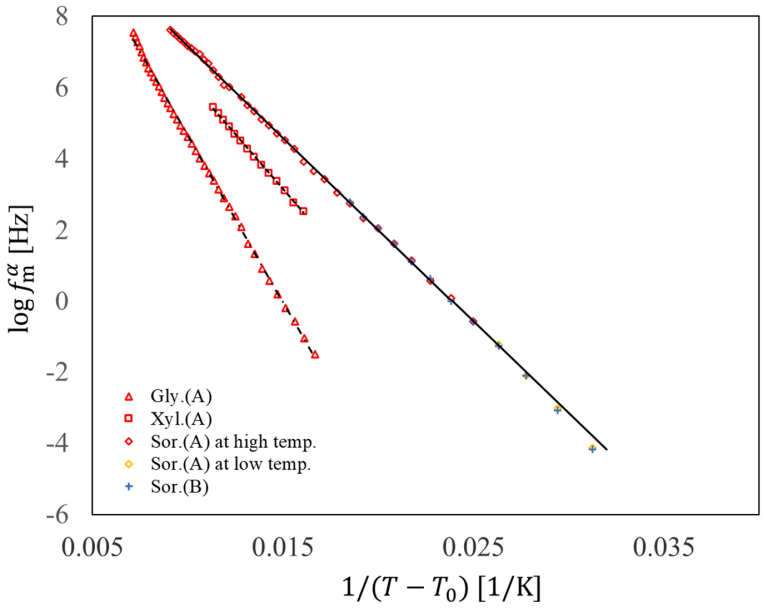

Figure 4.13: Relaxation map with fitting linees. Fitting for each materials. The parameters are shown in table 4.1. Sorbitol with a cooling rate of 0.7 K/min. is indicated by red symbols above 273 K and yellow symbols below 271 K.

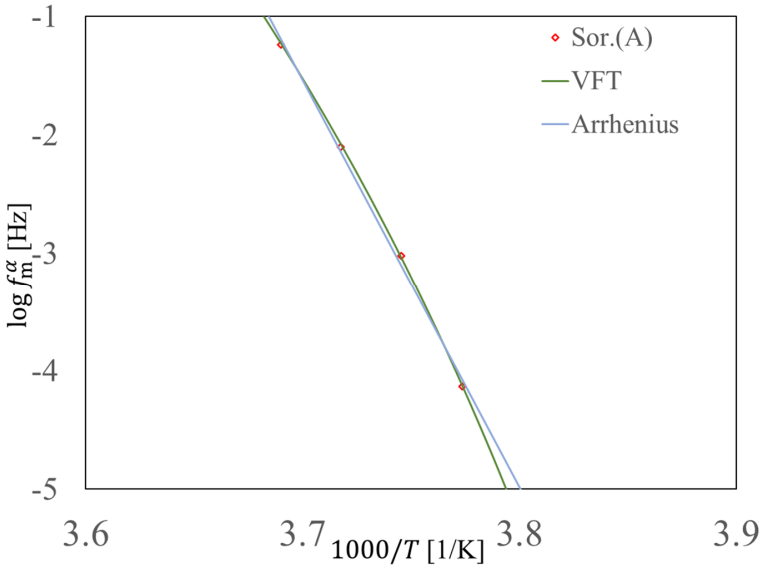

Figure 4.14: Fitting by arrhenius and VFT. This figure shows group-A sorbitol below 271 K with VFT and Arrhenius fitting curves. The solid line shows the fitting by the VFT equation with $A = 12.3, B = 460, T_0 = 237$ and Arrhenius type equation with $C = 126, D = 3.447$. The sum of squared residuals are 0.001 and 0.013 respectively.

From these results, we conclude that although theα process has divergent nature with respect to temperature, it is not so simple as f_{m}^{α} can be described by a single VFT equation. This suggests that slow dynamics such as α relaxation process near T_{g} requires somewhat new concepts in physics theories describing molecular motion. This may include a modified CRR development in AG theory. However, the required theories may have to affect to general slow dynamics including other that supercooled liquids.

Further investigation about this anomaly near T_{g} is necessary to understanding of the glass transition phenomena. We believe that measuring the quasi-equilibrium state of other samples or mixtures will help address this issue. In addition, when discussing the behavior of the α process near the glass transition temperature, it is necessary to clearly state the thermal history, such as cooling rate and waiting time after cooling.

Chapter 5

Conclusion and Summary

In this study, we focused on the α process, which is directly related to the glass transition phenomenon. It is known that the temperature dependence of the α process can be expressed by a non-arrhenius VFT equation. However, with the progress of measurement techniques, deviation of α relaxation frequency (or relaxation time) from the VFT equation near the glass transition temperature have been reported. This leads to the question of whether the glass transition is simply a relaxation phenomenon due to the finite observation time or some kind of transition.

On the other hand, these reports contain contradictory results. In order to measure quasi-equilibrium samples, it is necessary to pay attention to thermal history and other factors. However, previous studies have paid insufficient attention to such points. Therefore, we have performed dielectric spectroscopy over a wide frequency range using samples kept in quasi-equilibrium with sufficient attention to thermal history and so on for a precise discussion.

Although cells with fixed electrode spacing are commonly used to measure liquids, there is concern that negative pressure may occur as the temperature decreases. By using a movable cell, it was expected that the sample density would increase and the relaxation frequency would decrease compared to using a rigid-gap cell. The results of experiments with the movable-gap cell did not show the expected reduction in relaxation frequency and it had a large relaxation frequency compared to using the rigid-gap cell. The increase in relaxation frequency in movable-gap cell may be due to impurities. In addition, the effect of thermal history may have more influence on the relaxation frequency than the mobility of the cell.

It is known that the behavior of materials near the glass transition temperature changes depending on the thermal history. To measure samples in quasi-equilibrium, we used three types of sugar alcohols with low cooling rates and sufficiently long waiting times below the glass transition temperature as samples. The study was conducted on groups of samples with two different cooling rates, but no change in relaxation frequency was found between them. On the other hand, when we compared to the data with a cooling rate of 50 K/min., the samples with smaller cooling rates tend to have smaller relaxation frequency. Furthermore, all data for sorbitol could not be represented by a single VFT equation determined at the high temperature region, and data deviations from that equation were observed near the glass transition temperature. The results show a more drastic divergence trend than predicted by the VFT equation. The deviated data near the glass transition temperature were fitted with an Arrhenius-type equation and a VFT equation with different parameters. As a result, the VFT seems to represent the data better. This indicates that the divergence trend of relaxation frequency is still maintained near the glass transition temperature. These results suggest the requirement for a new physical theory to describe molecular motion such that it includes the modified CRR in AG theory. Furthermore, it is implied that glass transition is not simple relaxation phenomena and the dynamics may change near glass transition temperature.

Finally, we discuss future research directions. First, it would be useful to consider similarities or differences in deviations from the VFT in materials other than pure sorbitol. In the case of xylitol, there is the issue of difficulty in avoiding crystallization, but this may be solvable by measuring mixtures. Second, it may be useful to consider the molecular dynamics structural relaxation dynamics of molecular statistical ensemble which is introduced themolecular motion speed.

Chapter 6

Appendix

6.1 Relaxation parameters

Table 6.1: Relaxation parameters of 265 K sorbitol measured using different type of cells. Two measurements were made in each of these two cells.

Cell type (Measurement No.)	γ^{α}	δ^{α}	$\Delta\varepsilon^{\alpha}$	$\log f_{\mathrm{m}}^{\alpha}$	δ^{β}	$\Delta\varepsilon^{\beta}$	$\log f_{\mathrm{m}}^{\beta}$	ε_{∞}
rigid-gap cell(1)	0.6089	0.6662	37.65	-3.918	0.2731	7.251	3.840	3.243
rigid-gap cell(2)	0.5435	0.7022	36.64	-3.958	0.2992	6.636	3.927	3.507
movable-gap cell(1)	0.4588	0.7905	44.28	-3.827	0.2956	6.903	4.094	3.523
movable-gap cell(2)	0.5192	0.7762	46.84	-3.873	0.2525	8.125	4.125	2.902

Table 6.2: Relaxation parameters of group-A sorbitol. At 265 K, sample was measured five times with different pre-measurement waiting time.

Temp. [K]	γ^{α}	δ^{α}	$\Delta\varepsilon^{\alpha}$	$\log f_{\mathrm{m}}^{\alpha}$	δ^{β}	$\Delta\varepsilon^{\beta}$	$\log f_{\mathrm{m}}^{\beta}$	ε_{∞}
265 (142 h)	0.4600	0.8300	38.63	-4.093	0.3000	5.820	3.955	3.250
265 (379 h)	0.4600	0.8300	39.24	-4.138	0.3000	5.800	3.979	3.250
265 (816 h)	0.4600	0.8300	40.88	-4.100	0.3000	5.800	3.979	3.250

Temp. [K]	γ^{α}	δ^{α}	$\Delta\varepsilon^{\alpha}$	$\log f_{\mathrm{m}}^{\alpha}$	δ^{β}	$\Delta\varepsilon^{\beta}$	$\log f_{\mathrm{m}}^{\beta}$	ε_{∞}
265 (1075 h)	0.4600	0.8300	35.97	-4.095	0.3000	5.800	3.979	3.250
265 (1585 h)	0.4600	0.8300	38.12	-4.134	0.3000	5.800	3.979	3.250
267	0.4110	0.8070	33.29	-3.023	0.3150	6.140	4.063	3.250
269	0.4070	0.7850	33.89	-2.103	0.3290	6.540	4.132	3.250
271	0.4000	0.7850	33.42	-1.239	0.3600	6.280	4.285	3.600
273	0.3930	0.7760	34.14	-0.574	0.3740	6.900	4.359	3.600
275	0.4010	0.7620	30.03	0.100	0.3770	7.080	4.505	3.600
277	0.3940	0.7930	29.04	0.599	0.3880	7.800	4.567	3.600
279	0.3900	0.7920	30.22	1.169	0.3990	8.010	4.673	3.600
281	0.3950	0.8060	27.91	1.635	0.4150	8.010	4.858	3.600
283	0.3880	0.7930	28.68	2.062	0.4260	8.170	4.982	3.600
285	0.4020	0.7930	27.59	2.353	0.4340	8.870	5.005	3.600
287	0.3720	0.8000	27.67	2.758	0.4640	8.640	5.012	3.600
289	0.3610	0.8140	27.30	3.070	0.4730	8.450	5.071	3.600
291	0.3560	0.8000	27.18	3.435	0.4850	8.270	5.240	3.600
293	0.3450	0.8140	26.97	3.661	0.4920	8.060	5.384	3.600
295	0.3450	0.8290	26.47	3.926	0.5110	7.510	5.537	3.600
297	0.3260	0.8130	35.44	4.292	0.5630	7.71	5.776	2.500
299	0.3260	0.8130	35.05	4.531	0.6040	7.42	5.834	2.500
301	0.3390	0.8180	34.09	4.728	0.6200	7.29	6.006	3.000
303	0.3550	0.8000	33.16	4.951	0.6770	6.41	6.064	3.320
305	0.3450	0.8180	32.45	5.124	0.6770	6.31	6.119	3.320
307	0.3570	0.8080	33.33	5.344	0.6800	6.58	6.182	3.320
309	0.3770	0.8000	25.29	5.502	0.6840	6.410	6.320	3.320
311	0.4150	0.7400	29.81	5.737	0.6950	3.730	6.672	3.320
315	0.5690	0.6940	22.34	6.025	0.9180	2.100	6.727	5.050
317	0.5800	0.7770	22.45	6.067	0.8700	4.140	6.995	6.050
319	0.6450	0.7490	25.45	6.305	0.9440	2.720	7.349	6.050
321	0.7070	0.5770	19.02	6.497				5.250

Temp. [K]	γ^{α}	δ^{α}	$\Delta\varepsilon^{\alpha}$	$\log f_{\mathrm{m}}^{\alpha}$	δ^{β}	$\Delta\varepsilon^{\beta}$	$\log f_{\mathrm{m}}^{\beta}$	ε_{∞}
323	0.5470	0.7000	28.64	6.676				4.500
325	0.5150	0.7210	26.24	6.787				4.250
327	0.6120	0.7560	33.23	6.942				6.800
329	0.6240	0.7280	35.19	7.014				6.800
331	0.7310	0.7280	31.27	7.111				8.500
333	0.6700	0.8070	30.02	7.168				11.75
335	0.6700	0.7780	29.18	7.279				9.000
337	0.7010	0.7620	28.65	7.351				9.500
339	0.7010	0.7790	27.47	7.443				10.50
341	0.7180	0.7730	26.68	7.516				11.15
343	0.7430	0.7760	25.21	7.616				12.70

Table 6.3: Relaxation parameters of group-B sorbitol.

Temp. [K]	γ^{α}	δ^{α}	$\Delta\varepsilon^{\alpha}$	$\log f_{\mathrm{m}}^{\alpha}$	δ^{β}	$\Delta\varepsilon^{\beta}$	$\log f_{\mathrm{m}}^{\beta}$	ε_{∞}
265	0.5000	0.7920	39.77	-4.163	0.2950	6.090	3.892	3.000
267	0.4830	0.7350	34.08	-3.069	0.3180	5.900	4.081	3.000
269	0.4820	0.7360	33.66	-2.097	0.3180	6.880	4.106	3.200
271	0.4430	0.7610	32.89	-1.274	0.3600	6.630	4.320	3.700
273	0.4600	0.7560	32.81	-0.590	0.3300	3.710	4.337	3.700
275	0.4600	0.7380	30.06	-0.006	0.3610	8.370	4.349	3.700
277	0.4600	0.7380	28.86	0.645	0.3800	8.370	4.519	3.700
279	0.4600	0.7380	29.61	1.121	0.3800	9.160	4.551	3.700
281	0.4600	0.7380	28.36	1.614	0.3980	8.770	4.749	3.700
283	0.4600	0.7380	28.11	2.069	0.3980	-0.470	4.933	3.700
285	0.4600	0.7490	26.91	2.379	0.4300	9.470	4.976	3.700
287	0.4600	0.7490	26.29	2.801	0.4300	10.070	5.063	3.700

Table 6.4: Relaxation parameters of group-A xylitol.

Temp. [K]	γ^{α}	δ^{α}	$\Delta\varepsilon^{\alpha}$	$\log f_{\mathrm{m}}^{\alpha}$	δ^{β}	$\Delta\varepsilon^{\beta}$	$\log f_{\mathrm{m}}^{\beta}$	ε_{∞}
267	0.3757	0.8695	31.98	2.541	0.2387	115.083	-1.933	3.395
269	0.4627	0.7953	34.64	2.787	0.2844	18.052	2.683	3.544
271	0.3377	0.8776	34.39	3.123	0.4412	13.820	2.914	3.468
273	0.2848	0.9659	28.88	3.375	0.5005	17.382	3.468	3.267
275	0.3577	0.8638	38.10	3.604	0.5667	5.927	4.151	3.376
277	0.3460	0.8846	37.15	3.839	0.6138	6.145	4.438	3.217
279	0.3378	0.9000	35.87	4.068	0.6371	6.805	4.662	3.071
281	0.3257	0.9159	34.31	4.293	0.6538	7.821	4.848	2.856
283	0.3169	0.9243	32.53	4.503	0.6550	9.118	4.996	2.651
285	0.3094	0.9297	32.55	4.706	0.6893	8.496	5.197	2.284
287	0.3120	0.9231	30.79	4.910	0.6728	9.543	5.323	2.160
289	0.3043	0.9284	31.04	5.095	0.7080	8.395	5.514	1.703
291	0.3301	0.8941	31.43	5.286	0.7160	6.859	5.673	1.599
293	0.2726	0.9399	27.59	5.458	0.7005	9.921	5.734	0.574

Table 6.5: Relaxation parameters of group-A grycerol.

Temp. [K]	γ^{α}	δ^{α}	$\Delta\varepsilon^{\alpha}$	$\log f_{\mathrm{m}}^{\alpha}$	δ^{β}	$\Delta\varepsilon^{\beta}$	$\log f_{\mathrm{m}}^{\beta}$	ε_{∞}
193	0.9440	0.9580	43.68	-1.493	0.5280	3.690	0.5858	2.000
195	0.8950	0.9580	42.22	-1.052	0.6190	5.040	0.5858	2.000
197	0.8950	0.8840	43.07	-0.569	0.5590	5.040	0.9108	2.000
199	0.8950	0.8710	43.07	-0.205	0.5210	5.040	1.2938	2.000
201	0.8950	0.8980	39.92	0.215	0.5210	5.040	1.5378	2.000
203	0.8950	0.8980	39.92	0.599	0.5210	6.460	1.7198	2.000
205	0.7680	0.8630	39.45	0.929	0.6980	5.110	2.0171	2.500
207	0.7490	0.8400	28.95	1.354	0.3880	1.440	2.1218	2.500
209	0.9140	0.8080	31.96	1.639	0.4940	3.460	2.9648	2.500

Temp. [K]	γ^{α}	δ^{α}	$\Delta\varepsilon^{\alpha}$	$\log f_{\mathrm{m}}^{\alpha}$	δ^{β}	$\Delta\varepsilon^{\beta}$	$\log f_{\mathrm{m}}^{\beta}$	ε_{∞}
211	0.9140	0.8080	27.04	2.103	0.4940	3.180	3.1378	2.500
213	0.9140	0.8080	26.80	2.400	0.4940	3.570	3.2328	2.500
215	0.9300	0.8340	25.18	2.660	0.4940	3.780	3.4628	2.500
217	0.9300	0.8520	24.37	2.908	0.6070	3.780	3.9418	2.500
219	0.9300	0.8520	24.14	3.147	0.6070	3.780	4.1908	2.500
221	0.9540	0.8650	23.67	3.400	0.5690	3.530	4.6118	2.500
223	0.9000	0.8880	23.41	3.604	0.5920	3.530	4.8808	2.500
225	0.8390	0.8920	24.17	3.813	0.6270	2.450	5.2738	2.500
227	0.8390	0.8920	23.89	4.019	0.5220	2.330	5.4458	2.500
229	0.8390	0.8970	23.44	4.230	0.5220	2.330	5.3498	2.500
231	0.8390	0.8970	23.32	4.431	0.5220	2.330	5.5318	2.500
233	0.8390	0.9030	22.88	4.617	0.5220	2.330	5.7238	2.500
235	0.6810	0.9250	24.99	4.798				2.500
237	0.6810	0.9250	24.74	4.952				2.500
239	0.6810	0.9350	24.12	5.122				2.500
241	0.6810	0.9350	23.63	5.266				2.500
243	0.6910	0.9350	22.88	5.433				2.500
245	0.6910	0.9350	22.14	5.567				2.500
247	0.6910	0.9350	21.02	5.725				2.500
249	0.6910	0.9350	19.66	5.888				2.500
251	0.6910	0.9350	17.83	6.029				2.500
253	0.6910	0.9350	15.74	6.168				2.500
255	0.6910	0.9350	13.44	6.302				2.500
257	0.6820	0.9350	10.95	6.427				2.500
259	0.6680	0.9450	9.03	6.554				2.500
261	0.5800	0.9450	7.55	6.716				2.100
263	0.5800	0.9450	6.29	6.852				2.200
265	0.5380	0.9450	5.03	7.006				2.200
267	0.5160	0.9450	4.32	7.168				2.200

Temp. [K]	γ^{α}	δ^{α}	$\Delta\varepsilon^{\alpha}$	$\log f_{\mathrm{m}}^{\alpha}$	δ^{β}	$\Delta\varepsilon^{\beta}$	$\log f_{\mathrm{m}}^{\beta}$	ε_{∞}
269	0.5210	0.9450	4.14	7.284				2.200
271	0.4770	0.9450	4.38	7.432				1.950
273	0.4770	0.9450	4.65	7.537				1.850

Table 6.6: Relaxation parameters of group-B grycerol.

Temp. [K]	γ^{α}	δ^{α}	$\Delta\varepsilon^{\alpha}$	$\log f_{\mathrm{m}}^{\alpha}$	δ^{β}	$\Delta\varepsilon^{\beta}$	$\log f_{\mathrm{m}}^{\beta}$	ε_{∞}
193	0.6110	0.9460	63.71	-1.506	0.2460	0.647	2.304	2.485

Chapter 7

Acknowledgement

I would like to thank my supervisor Prof. Ryusuke Nozaki for support my work. I would like to express my appreciation to Prof. Tomobumi Mishina, Prof. Koji Nemoto and Prof. Tadaaki Nagao for valuable comments. I appreciate the encouragement of the member of the condenced matter physics group. This work was supported by JST SPRING, Grant Number JPMJSP2119 and JSPS KAKENHI, Grant Number JP19K03759.

References

[1] H. Vogel. Das temperaturabhaengigkeitsgesetz der viskositaet von fluessigkeiten. *Physikalische Zeitschrift*, 22:645–646, 1921.

[2] G. Fulcher. Analysis of recent measurements of the viscosity of glasses. *Journal of the American Ceramic Society*, 8, 1925.

[3] G. Tammann and W. Hesse. Die abhangigkeit der viscositat von der temperatur bie unterkuhlten flussigkeiten. *Z Anorg Allg Chem*, 156, 1926.

[4] Malcolm L. Williams, Robert F. Landel, and John D. Ferry. The temperature dependence of relaxation mechanisms in amorphous polymers and other glass-forming liquids. *Journal of the American Chemical Society*, 77, 1955.

[5] G. Adam and J. Gibbs. On the temperature dependence of cooperative relaxation properties in glass-forming liquids. *J. Chem. Phys.*, 43(1):139–146, 1965.

[6] S. Matsuoka. *Relaxation Phenomena in Polymers*. Oxford University Press, 1992.

[7] M. Nakanishi and R. Nozaki. Systematic study of the glass transition in polyhydric alcohols. *Phys. Rev. E Stat. Nonlin. Soft. Matter Phys.*, 83, 2011.

[8] M. Nakanishi and R. Nozaki. High-frequency broadband dielectric spectroscopy on sugar alcohols below tg. *J. Non. Cryst. Solids*, 356, 2010.

[9] M. Nakanishi and R. Nozaki. Dynamics and structure of hydrogen-bonding glass formers: Comparison between hexanetriol and sugar alcohols based on dielectric relaxation. *Phys. Rev. E Stat. Nonlin. Soft. Matter Phys.*, 81, 2010.

[10] A. Minoguchi Y. Yomogida and R. Nozaki. Ultraslow dielectric relaxation process in supercooled polyhydric alcohols. *Phys. Rev. E*, 73:041510, 2006.

[11] K. Kitai A. Minoguchi and R. Nozaki. Difference and similarity of dielectric relaxation processes among polyols. *Phys. Rev. E*, 68:031501–1–031501–7, 2003.

[12] Ayumi Minoguchi R. Nozaki, Hiroomi Zenitani and Kei Kitai. Dielectric relaxation processes in water-in-sorbitol mixtures. *J. Non-Cryst. Solids*, 307-310:349–355, 2002.

[13] H. Sotokawa A. Minoguchi, T. Kaneko and R. Nozaki. Dielectric relaxation processes in supercooled polyhydric alcohols and their mixtures. *J. Non-Cryst. Solids*, 352, 2006.

[14] S. Ozawa R. Nozaki, D. Suzuki and Y. Shiozaki. The α and the β relaxation processes in supercooled sorbitol. *J. Non-Cryst. Solids*, 235-237:393–398, 1998.

[15] R. Nozaki and S. Mashimo. Dielectric relaxation measurements of poly(vinyl acetate) in glassy state in the frequency range $10^{-6} - 10^{6}$Hz. *J. Chem. Phys.*, 87(4):2271–2277, 1987.

[16] J. Zhao and G. B. McKenna. Temperature divergence of the dynamics of a poly(vinyl acetate) glass: Dielectric vs. mechanical behaviors. *J. Chem. Phys*, 136:154901, 2012.

[17] C. A. Angell and D. L. Smith. Test of the entropy basis of the vogel-tammann-fulcher equation. dielectric relaxation of polyalcohols near tg. *J. Chem. Phys*, 86(19):3845–3852, 1982.

[18] B. N. Olsen T. Hecksher, I. A. Nielsen and C. J. Dyre. Little evidence for dynamic divergences in ultraviscous molecular liquids. *Nat. Phys.*, 4, 2008.

[19] G. B. McKenna. Diverging views on glass transition. *Nat. Phys.*, 4, 2008.

[20] S. L. Simon J. Zhao and G. B. McKenna. Using 20-million-year-old amber to test the super-arrhenius behaviour of glass-forming systems. *Nat. Comm.*, 2809:1–6, 2013.

[21] V. N. Novikov and A. P. Sokolov. Temperature dependence of structural relaxation in glass-forming liquids and polymers. *Entropy*, 24, 2022.

[22] Flow, diffusion and crystallization of supercooled liquids: Revisited. *Journal of Chemical Physics*, 112, 2000.

[23] K. L. Ngai. *Relaxation and Diffusion in Complex Systems*. Springer, 2011.

[24] D. J. Ferry. *Viscoelastic properties of polymers. Viscoelastic properties of polymers*. 1980.

[25] A J Kovacs. La contraction isotherme du volume des polym 竪res amorphes. *Journal of Polymer Science*, 30, 1958.

[26] J. M. Hutchinson and A. J. Kovacs. Simple phenomenological approach to the thermal behavior of glasses during uniform heating or cooling. *J Polym Sci Part A-2 Polym Phys*, 14, 1976.

[27] H. Frohlich. *Theory of Dielectrics Dielectric Constant and Dielectric Loss*. Oxford at the Clarendon Press, 1960.

[28] F. Krmer and A. Schonhals. *Broadband Dielectric Spectroscopy*. Springer, 2003.

[29] Denkigakkai. *Denkigakkaidaigakukoza Yudentaigenshoron (Dielectric Phenomenology written in Japanese)*. Denkigakkai, 1973.

[30] Kenneth S. Cole and Robert H. Cole. Dispersion and absorption in dielectrics i. alternating current characteristics. *The Journal of Chemical Physics*, 9, 1941.

[31] D. W. Davidson and R. H. Cole. Dielectric relaxation in glycerine, 1950.

[32] S. Havriliak and S. Negami. A complex plane representation of dielectric and mechanical relaxation processes in some polymers. *Polymer*, 8, 1967.

[33] M. Nakanishi, Y. Sasaki, and R. Nozaki. New sample cell configuration for wide-frequency dielectric spectroscopy: Dc to radio frequencies. *Review of Scientific Instruments*, 81, 2010.

[34] F. Alvarez, A. Alegra, and J. Colmenero. Relationship between the time-domain kohlrausch-williams-watts and frequency-domain havriliak-negami relaxation functions. *Physical Review B*, 44, 1991.

[35] U. Schneider, P. Lunkenheimer, R. Brand, and A. Loidl. Dielectric and far-infrared spectroscopy of glycerol. *Journal of Non-Crystalline Solids*, 235-237, 1998.